Biochemical Pharmacology 242 (2025) 117424

Contents lists available at ScienceDirect

Biochemical Pharmacology

journal homepage: www.elsevier.com/locate/biochempharm

Discovery of SERCA1-specific small molecule inhibitors based on survival mechanisms in metastatic hepatocellular carcinoma cells that depend on CaMK2α-mediated SERCA1 expression

Jin Hong Lim [a], Keunwan Park [b], Kyung Hwa Choi [c], JungMin Kim [d], Yoo-Lim Jhe [d], Seok-Mo Kim [a], Ki-Cheong Park [d,*], Jae-Ho Cheong [d,e,f,g,h,**]

[a] Gangnam Severance Hospital, Department of Surgery, Yonsei University College of Medicine, 211 Eonjuro, Gangnam-gu, Seoul 06273, Republic of Korea
[b] Natural Product Informatics Research Center, KIST Gangneung Institute of Natural Products, Gangneung 25451, Republic of Korea
[c] Department of Urology, CHA Bundang Medical Center, CHA University, Seongnam 13496, Republic of Korea
[d] Department of Surgery, Yonsei University College of Medicine, 50-1, Yonsei-ro, Seodaemun-gu, Seoul 03722, Republic of Korea
[e] Severance Biomedical Science Institute, BK21 PLUS Project for Medical Science, Yonsei University College of Medicine, Republic of Korea
[f] Brain Korea 21 Project for Medical Science, Yonsei University College of Medicine, Republic of Korea
[g] YUMC-KRIBB Medical Convergence Research Institute, Yonsei University College of Medicine, Republic of Korea
[h] Department of Biochemistry & Molecular Biology Yonsei University College of Medicine, Republic of Korea

ARTICLE INFO

Keywords:
Patient-derived metastatic HCC
Sarcoplasmic
Endoplasmic reticulum calcium ATPase
Calcium
Calmodulin-dependent protein kinase 2 alpha

ABSTRACT

Refractory hepatocellular carcinoma (HCC) perpetuates metastasis or recurrence through anti-cancer drug resistance, necessitating more effective and reliable therapeutic strategies. We propose a new therapeutic approach involving the discovery of novel small molecules through target identification and validation in a patient-derived metastatic HCC model. We showed that calcium/calmodulin-dependent protein kinase 2 alpha (CaMK2α)-mediated enhancement of sarco/endoplasmic reticulum (ER) calcium ATPase 1 (SERCA1) expression level was pivotal events under anti-cancer drug treated conditions in patient-derived metastatic HCC cells. Increased SERCA1 was regulates to overloaded free calcium. SERCA is widely recognized as a key regulator of cytosolic free calcium under severe ER stress conditions. Though a cardiac dysfunction was unavoidable in vivo because of non-specific inhibition of SERCA isoforms by standard SERCA inhibitors. Based on the molecular structure of SERCA1, we discovered and synthesized two SERCA1-specific inhibitors, candidate 56 and 62. These compounds significantly reduced tumor size in the metastatic HCC xenograft tumor model without cardiac contractile dysfunction. This study first showed survival mechanism of patient-derived metastatic HCC cell, and propose a new therapeutic approach by the new small molecules, candidate 56 and 62, which are SERCA1 isoform-specific inhibitors without cardiac dysfunction by SERCA1 selectively inhibition.

1. Introduction

Hepatocellular carcinoma (HCC) is a well-known form of liver cancer, comprising over 90 % of hepatic carcinoma cases. Fortunately, advancements in systemic treatments for advanced HCC have led to a steady increase in patient survival rates [1]. However, the emergence of anti-cancer drug resistance in some cases presents a critical challenge, leading to patient mortality due to cancer recurrence and metastasis [2]. Molecular variations suggest the poor prognosis of HCC in patients with metastasis or recurrence; however, the fundamental mechanisms remain unclear. Therefore, more efficient and reliable therapeutic approaches are required. Recently, the ratio of relapse to survival after surgery was

Abbreviations: SERCA, sarco/endoplasmic reticulum calcium ATPase; CaMK2α, Calcium/calmodulin-dependent protein kinase alpha; NFκB, nuclear factor kappa B; RNA-Seq, RNA sequencing; qRT-PCR, quantitative reverse transcription PCR; CSCs, cancer stem cells; ER, endoplasmic reticulum; siRNA, small interfering RNA; RPMI-1640, Rosewell Park Memorial Institute-1640; FBS, Fetal Bovine Serum; YUMC, Yonsei University Medical Center.

* Corresponding author at: Department of Surgery, Yonsei University College of Medicine, 50-1, Yonsei-ro, Seodaemun-gu, Seoul 120-752, Republic of Korea.
** Corresponding author at: Department of Surgery, Department of Biochemistry & Molecular Biology, Systems Cancer Biology & Biomarker Research Lab, Yonsei University College of Medicine, Seoul, Republic of Korea.
E-mail addresses: ggiru95@yuhs.ac (K.-C. Park), jhcheong@yuhs.ac (J.-H. Cheong).

https://doi.org/10.1016/j.bcp.2025.117424
Received 16 September 2025; Received in revised form 8 October 2025; Accepted 9 October 2025
Available online 12 October 2025

determined following systemic chemotherapy before surgery, regardless of cancer development [3]. Systemic chemotherapy is typically administered to patients with advanced cancer subtypes characterized by invasion or metastatic lesions, as local therapies are often inadequate against chemotherapy-resistant cancer [4,5]. Anti-cancer drug treatments exert significant stress on cancer cells, contributing to cellular viability challenges. Cancer stem cells (CSCs) have demonstrated resilience against metabolic stresses within tumor microenvironments through epigenetic reprogramming, emerging as a notable therapeutic target [6]. Under anti-cancer drug treatment conditions, CSCs exhibit enhanced survival mechanisms against acute sarco/endoplasmic reticulum (ER) stress compared to non-CSCs, prompting the exploration of various molecular strategies for epigenetic reprogramming [7]. Epigenetic reprogramming stimulated by anti-cancer drugs may involve several molecular regulators [8,9]. Previous studies have established calcium/calmodulin-dependent protein kinase alpha (CaMK2α) as a pivotal transcriptional regulator that inhibits cytosolic free calcium-mediated apoptosis by upregulating sarco/ER calcium ATPase (SERCA) levels [9]. Furthermore, CaMK was a key transcriptional regulator of increased peroxisome proliferator-activated receptor gamma coactivator 1-alpha (PGC-1α) expression, which is a potent inducer of ATP production via mitochondrial respiration [10]. Cytosolic free calcium levels play a critical role in cellular responses to ER stress and subsequent cell fate decisions [11]. ER stress causes the release of cytosolic free calcium from the ER to the cytosol via IP3R (inositol 1,4,5-trisphosphate) receptors, which is regulated by calcium pumps, exchangers, and channels to maintain cellular calcium homeostasis [12]. Excessive elevation of cytosolic free calcium beyond physiological levels triggers apoptotic signals [13]. SERCA serves as a key regulator in managing overloaded cytosolic free calcium levels in cancer cells, contributing to cellular defense by efficiently restoring cytosolic free calcium to the ER [14–16]. Previously, we showed potential implications for applying new combinatorial strategies and discovering anti-cancer candidates that SERCA-targeted a specific vulnerability of anti-cancer drug-resistant-mediated cells [17]. However, a cardiac dysfunction was unavoidable in xenograft model because of non-selective inhibition of SERCA isoforms by several candidates [17,18]. Injured myocardial calcium cycling is a key regulator of heart failure (cardiac dysfunction), causing to a change in the structure remodelling and contractile function of the heart [19]. In cardiomyocytes, the regulation of cytosolic free calcium storage and release by sarcoplasmic reticulum (SR) is mostly dependent on calcium regulation proteins, such as SERCA2a. For the relaxation phase of the cardiac cycle, SERCA2a is a pivotal regulator in transporting cytosolic free calcium back to the SR, to restore cytosolic free calcium levels to their resting state and replenish SR calcium levels for the next contraction. However, functional inhibition of SERCA2a by thapsigargin (non SERCA isoform specific inhibitor) causes to cardiac dysfunction [20]. The current study purposed to design a therapeutic approach with diminish of cardiac dysfunction based on CaMK2α-mediated enhancement of SERCA1 via the regulation of cytosolic free calcium levels. We further aimed to identify targets and novel small molecules for isoform-specific inhibition of metastatic HCC under acute ER stress in patient-derived samples. The outcomes of this study are clinically significant for the development of new small molecules with decrease of side effects that selectively and effectively target highly malignant cancer cells, including cancer stem-like cells and drug-resistant cancer cells.

2. Materials and methods

2.1. Patient characteristics

The patients recruited for current research underwent liver resection. The patients were treated between from January 2018 to December 2022 at the Severance Hospital (Seoul, South Korea). The study protocol was approved by the Institutional Review Board (IRB) of Severance Hospital, Yonsei University College of Medicine (IRB protocol: 3–2022-0331). Cell samples were obtained from the patients at the Severance Hospital, Yonsei University College of Medicine, Seoul, Korea. Further details of the protocol have been previously published [8].

2.1.1. Patient 1

YUMC-NM-H1 is a 71-year-old woman diagnosed with hepatocellular carcinoma (HCC). She presented with a 2.5 cm multinodular-confluent HCC located in segment 3 of the liver. She underwent a left lateral sectionectomy. The postoperative pathology confirmed HCC with clear resection margins. During routine follow-up examinations, including radiological studies and serum tumor markers (alpha-fetoprotein), no evidence of recurrence was observed.

2.1.2. Patient 2

YUMC-M−H1 is a 53-year-old woman diagnosed with hepatocellular carcinoma (HCC). She had a 9 cm multinodular, confluent HCC involving the left liver lobe and the hilar bile duct. She underwent left trisectionectomy and radical resection of the common bile duct in October 2018. During subsequent follow-up, recurrence was detected in the omentum and lung. She was treated with sorafenib; however, tumor progression was also noted in the lungs. The chemotherapy regimen was subsequently switched to regorafenib. In June 2019, recurrence was limited to the omentum, with lung metastasis remaining stable. She subsequently underwent excision of an abdominal wall mass in June 2019.

2.1.3. Patient 3

YUMC-M−H2 is a 67-year-old man diagnosed with hepatocellular carcinoma (HCC). He presented with a 2 cm tumor in the right lobe of the liver and underwent right hemihepatectomy in February 2018. Twelve months postoperatively, metastasis to the right diaphragm was identified during routine follow-up. In April 2019, he underwent wide excision of the diaphragmatic mass. Following this, he received sorafenib chemotherapy for 11 months. In February 2020, further recurrence was noted in the diaphragm and omentum. He then underwent wide excision of the diaphragm and omentectomy.. Postoperatively, he received a third line of chemotherapy with 5-FU and cisplatin between March 2020 and August 2021. Due to multiple subsequent recurrences involving segment 4 of the liver, the mesentery around the transverse colon, and the retroperitoneum near the right adrenal gland, chemotherapy was discontinued. In March 2022, he underwent wedge resection of segment 4 of the liver, segmental resection of the colon, and retroperitoneal resection. Culture specimens obtained during this procedure confirmed the histopathological diagnosis of HCC. The patient subsequently ceased hospital visits and follow-up was discontinued.

2.1.4. Patient 4

YUMC-M−H3 is a 71-year-old man diagnosed with hepatocellular carcinoma (HCC). He presented 2 cm tumor in the right lobe of the liver and underwent right anterior sectionectomy in February 2019. three months postoperatively, metastasis to the lymph node was identified during routine follow-up. He was treated with concurrent chemoradiation therapy (5-FU and cisplantin). After evaluating the response, he underwent lymph node dissection in January 2020. Postoperative culture specimens were obtained. The patient has since been regularly followed up in the outpatient department.

2.2. Patient tissue specimens

Tumor specimens were obtained from patients with histologically and biochemically confirmed recurrent or metastatic tumors who were medicated at Severance Hospital, Yonsei University College of Medicine, Seoul, Korea. Fresh tumor specimens were obtained for surgical resection.

2.3. Ethical considerations

Current study protocol was confirmed by the Institutional Review Board of Severance Hospital, Yonsei University College of Medicine (Institutional Review Board Protocol: 3–2022-0331). Samples were obtained from patients at Severance Hospital, Yonsei University College of Medicine, Seoul, South Korea. The requirement for obtaining formal written consent was waived owing to the retrospective observational nature of the study.

2.4. Tumor cell isolation and primary culture

After excision, the tumors were kept in normal saline containing antifungal agents and shifted to the laboratory. Fat and normal tissues were eliminated, and the tissues were washed with 1 × Hank's Balanced Salt Solution. The cells were resuspended in Rosewell Park Memorial Institute (RPMI)-1640 medium (Hyclone, South Logan, UT, USA) with 20 % FBS (Hyclone) and 2 % penicillin/streptomycin solution (Gibco, Grand Island, NY, USA). Further details of the protocol have been previously published [8].

2.5. Cell culture

The patient-derived cancer cells and THLE-2, Huh-7, HepG2, Hep3B cells were obtained from fresh tumors of patients or ATCC (ATCC, Manassas, VA, USA). YUMC-NM-H1 (non-metastatic HCC) and YUMC-M−H1, –H2, and –H3 (metastatic HCC) cells were isolated from patients with HCC treated at the Severance Hospital, Yonsei University College of Medicine, Seoul, Korea. Cells were grown in RPMI-1640 medium containing 20 % FBS. Cells were authenticated using short tandem repeat profiling, karyotyping, and isoenzyme analysis. Mycoplasma contamination was evaluated using a Lookout Mycoplasma PCR Detection Kit (Sigma-Aldrich, St. Louis, MO, USA; MP0035).

2.6. mRNA sequencing and analysis

Whole RNA was segregated from the patient-derived cancer cells, YUMC-NM-H1 (non-metastatic HCC) and YUMC-M−H1, –H2, and –H3 (metastatic HCC), using TRIzol Reagent (Thermo Fisher Scientific, Waltham, MA, USA) following to the manufacturer's instructions. Paired-end sequencing reads were generated on the Illumina sequencing NovaSeqX platform. Before starting analysis, Trimmomatic v0.38 was used to remove adapter sequences and trim bases with poor base quality. RNA enrichment (total RNA) in current study, we preprocessed the raw reads from the sequencer to remove low quality and adapter sequences before analysis and aligned the processed reads to the *Homo sapiens* genome assembly (GRCh38) using HISAT v2.1.0 (HISAT2, RRID: SCR 015530) [21]. Further details of the protocol have been previously published [22].

2.7. Statistical analysis of gene expression level

The relative amounts of genes were estimated in Read Count with StringTie. We carried out statistical analyses to discover conditionally expressed genes with the estimates of prevalence for each gene in the samples. Statistical analysis in current study was used raw p-value instead to FDR. Because if used FDR, not acquired sufficiently gene list for analysis of enrichment for GO and KEGG. For differentially expressed genes (DEGs) sets, hierarchical clustering analysis was carried out with complete linkage and Euclidean distance as a calculate of similarity. Gene-enrichment and functional annotation analysis and pathway analysis for statistically significant genes were carried out based on KEGG pathway and Gene Ontology analyses. Further details of the protocol have been previously published [8].

2.8. siRNA transfection for CaMK2α knockdown

Patient-derived metastatic HCC cells, YUMC-M−H1, –H2, and –H3 cells were transfected with CaMK2α siRNA or scrambled control siRNA. Sequence of the CaMK2α siRNA was designed using si-Designed software (Bioneer, Daejeon, South Korea) and the siRNA duplex was purchased from Bioneer. The sense and antisense sequences of the siRNA were as follows: 5′-UGAUCGAA GCCAUAAGCAA(dTdT)-3′ (forward) and 5′-UUGCUUAUGGCUUCGAUCA(dTdT)-3′ (reverse). Further details are provided in our previously published article [9].

2.9. Subcellular fractionation and immunoblot analysis

Primary antibodies against GPC3 (1:500, Cat#174851, Abcam, Cambridge, UK), HSP70 (1:500, Cat#2787, Abcam), TP (1:500, Cat#226917, Abcam), SERCA1 (1:200, Cat#133275, Abcam), SERCA2 (1:400, Cat#137020, Abcam), SERCA3 (1:200, Cat#154259, Abcam), Bcl-2 (1:400, Cat#196495, Abcam), pCaMK2α (1:500, Cat#171095, Abcam), CaMK2α (1:500, Cat#92332, Abcam), pIKKα (1:500, Cat#138426, Abcam), CHOP (1:500, Cat#7351, Santa Cruz Biotechnology, CA, USA), pNFκB (1:500, Cat#86299, Abcam), Histone H3 (1:500, Cat#18521, Abcam), caspase-3 (1:500, Cat#9661, Cell Signaling Technology, Beverly, MA,USA) and β-actin (1:500, Cat#47778) were used. Equal amounts of protein were separated on an 8–10 % sodium dodecyl sulfate–polyacrylamide gel, and the resolved proteins were electrotransferred onto polyvinylidene fluoride membranes (Millipore, Bedford, MA, USA). Nuclear fractions were performed with NE-PER Nuclear and Cytoplasmic Extraction reagents (Thermo Fisher Scientific; #78833) following the manufacturer's manuals. Separated cytoplasmic and nuclear extracts were isolated with a protein extraction solution (PRO-PREP, iNtRON Biotechnology, Seoul, Korea, #17081) or a histone extraction kit (Abcam, Cambridge, UK, #113476). Further details of the protocol have been previously published [8].

2.10. Electrophoretic mobility shift assay (EMSA)

The DNA binding affinity of NFκB against the SERCA1 promoters was verified with a ^{32}P-labeled oligonucleotide. Specific unlabelled and labeled oligonucleotides are as follows. Nuclear extracts were isolated with NE-PER Nuclear Extraction Reagents (Pierce, Rockford, IL, USA; 78833) and total lysate extraction solution (PRO-PREP, iNtRON Biotechnology, Seoul, Korea, 17081). The DNA binding affinity of NFκB against the *SERCA1* promoter was verified with a ^{32}P-labeled oligonucleotide. unlabeled and labeled oligonucleotides specific for NFκB (Forward 5′-GGGGGGTTCCC-3′, Reverse 5′-GGGAACCCCCC-3′) and mutant NFκB (Forward 5′-GGGcGcTTCCC-3′, Reverse 5′-GGGAAgCgCCC-3′) were synthesized by Bioneer. Further details of the protocol have been previously published [8].

2.11. Dual luciferase reporter assay

Promoter affinity was estimated with the Dual-Luciferase Reporter Assay (Promega, Madison, WI, USA; E1960), following the manufacturer's protocol. Regions of NFκB binding sites were amplified by PCR from human genomic DNA (NFκB primers: Forward 5′-GGGGGGTTCCC-3′, Reverse 5′-GGGAACCCCCC-3′). The PCR products were cloned into the pGL4.70 promoter Vector (Promega) using T4 DNA ligase (Thermo Scientific, Waltham, MA, USA; EL0011). All insertions were confirmed by sequencing.

2.12. Immunofluorescence analysis and confocal imaging

Nuclear translocated pNFκB level was estimated by immunofluorescence staining. Cells cultured on glass-bottomed dishes (MatTek, Ashland, MA. USA) were fixed with 4 % formaldehyde solution (R&D Systems, Abingdon, UK) for 10 min. Allslides were incubated with

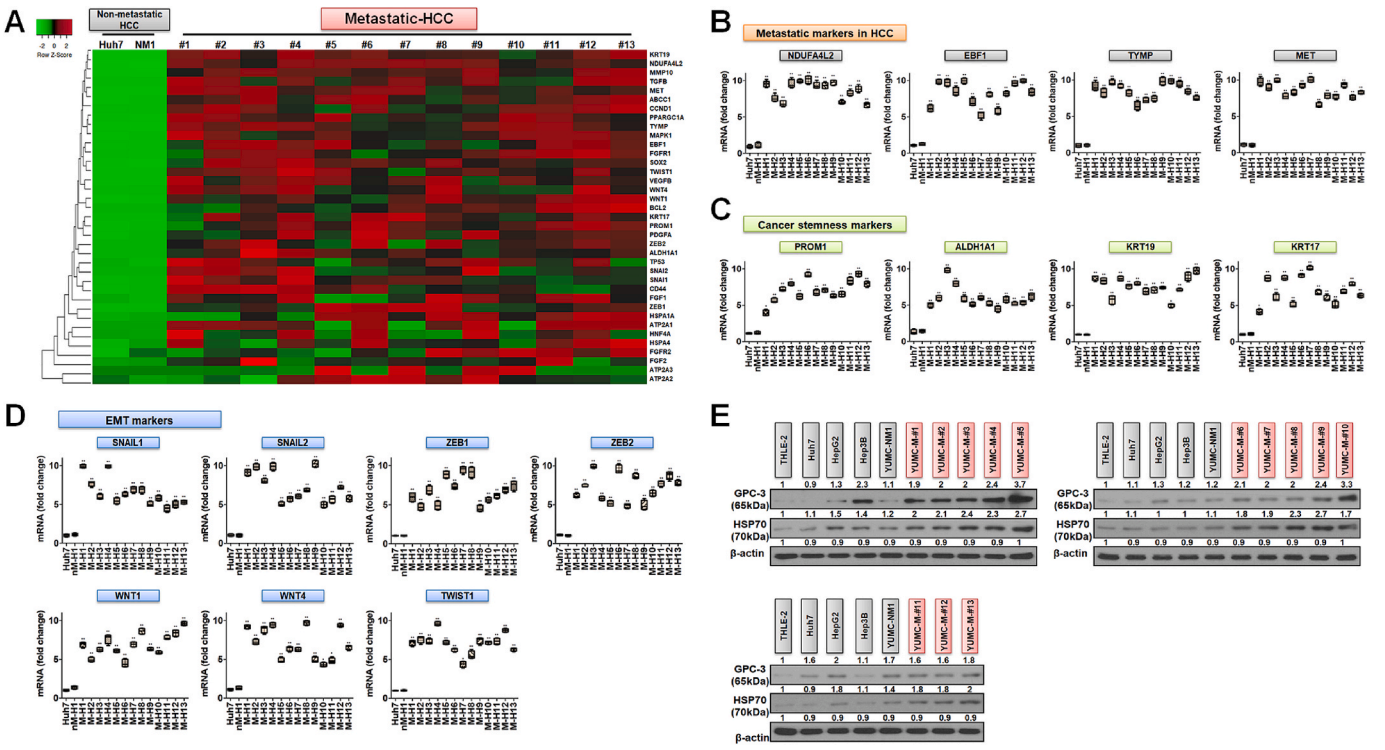

Fig. 1. Target gene expression profiling in patient-derived metastatic HCC. A, Hierarchical clustering shows differential gene expression; gene expression profiles in the patient-derived non-metastatic HCC (n = 1, female) and metastatic HCC cells (n = 13, male; 9, female; 4) compared to those in established HCC, Huh7. B–D, Gene expression variances were evaluated on mRNA sequencing (mRNA seq) analysis between the non-metastatic and metastatic HCC cells. E, Immunoblot analysis for expression of HCC markers between the non-metastatic and metastatic HCC cells compare than normal liver cell. **; $p < 0.01$ versus non-metastatic HCC cells.

secondary antibody, Alexa 488 (1:200; Molecular Probes, Eugene, OR, USA) for2 hours at room temperature. Nuclei were stained with Hoechst 33,342 (Life Technologies) for visualization. Images were obtained under a confocal microscope (LSM Meta 700; Zeiss, Oberkochen, Germany) and analyzed with the Zeiss LSM Image Browser, version 4.2.0121.

2.13. Cytosolic free calcium measurements using microspectrofluorimetry

Cytosolic free calcium levels in patient-derived HCC cells were detected with a calcium-sensitive fluorescent dye, Fura-2AM. HCC cells were incubated with Fura-2AM in normal phosphate-buffered saline (PBS) solution for 30 min at 37 ℃, followed by de-esterification of the dye for another 30 min at 22–25 ℃. Further details are provided in a previously published article [8].

2.14. Cell viability assay

Cell viability was estimated with the 3-(4,5-dimethylthiazol-2-yl)-2,5-diphenyltetrazolium bromide) assay. Cells were cultured in 96-well plates at 6×10^3 cells per well and cultured overnight to 80 % confluency. Further details on the protocol are available in existing publications [8,9,23]. The assay was conducted thrice and cell viability was measured as a percentage of the signal detected in vehicle-treated cells and documented as the means ± standard error of the mean.

2.15. Molecular docking simulation for SERCA1

The three-dimensional structure of SERCA1 was prepared using AlphaFoldDB [24] with the UniProt ID O14983. Most of the residues in the alpha-fold-predicted structure had high confidence scores, confirming reliability of the prediction model. The modeled human SERCA1 structure was further refined using Rosetta Relax [25] for use in subsequent docking simulations to elucidate crucial ligand-receptor interactions. The docking simulations for the two active compounds were conducted using DiffDock, which exhibits superior performance in blind docking tasks (i.e., docking simulation without knowing prior binding site information) The docked complex model was refined using RosettaLigand by performing iterative local docking refinement and energy minimization [26]. The final docking model was selected based on the interface binding energy (interface delta score) and used to analyze detailed molecular interactions.

2.16. Total RNA extraction and quantitative reverse transcription-polymerase chain reaction

Total RNA was isolated from tumor cells with the RNeasy Mini Kit (Qiagen, cat. 74106) and One-Step reverse transcription-polymerase chain reaction (RT-PCR) Kit (Qiagen, Cat#204243) folowing manufacturer's protocols. Whole data were normalized to *α-tubulin*. *SERCA1, SERCA2,* and *SERCA3* primers were used for quantitative RT-PCR (qRT-PCR) analysis: *SERCA1*, 5′-GTGATCCGCCAGCTAATG-3′ (forward) and 5′-CGAATGTCAGGTCCGTCT-3′ (reverse); *SERCA2*, 5′-GGTGGTTCA TTGCTGCTGAC-3′ (forward) and 5′-TTTCGGACAAGCTGTT GAGG-3′ (reverse); *SERCA3*, 5′-GATGGAGTGAACGACGCA-3′ (forward) and 5′-CCA GGTATCGGAAGAAGAG-3′ (reverse); and α-tubulin; 5′-CGGGCAGTGTTTGTAGACTTGG-3′ (forward) and 5′-CTCCTTGCC AATGGTGTAGTGC-3′ (reverse).

2.17. In vivo mouse xenograft model with patient-derived HCC cells

All the experiments were carried out in accordance with the guidelines established by the Animal Experimentation Committee of Yonsei University. Patient-derived HCC cells (4.5×10^6 cells/mouse) were injected subcutaneously into the upper left flank region of female NOD/Shi-scid, IL-2Rγ KOJic mice. After 13 days, the tumor cell-planted mice

Table 1
Properties and clinical features of 14 patients. Patient-derived Hepatocellular carcinoma cells were isolated from these patient specimen.

	YUMC-NM-H1	YUMC-M−H1	YUMC-M−H2	YUMC-M−H3	YUMC-M−H4	YUMC-M−H5	YUMC-M−H6	YUMC-M−H7	YUMC-M−H8	YUMC-M−H9	YUMC-M−H10	YUMC-M−H11	YUMC-M−H12	YUMC-M−H13
Age at Diagnosis	71	66	67	67	66	51	53	47	61	63	49	65	53	71
Gender	Female	Male	Male	Male	Male	Male	Female	Female	Male	Male	Male	Male	Female	Male
Primary Disease Site	Liver	Liver	Liver	Liver	Liver	Liver	Liver	Liver	Liver	Liver	Liver	Liver	Liver	Liver
Primary Pathology	Hepato cellular carcinoma	Hepatocellular carcinoma (metastasis)	Hepato cellular carcinoma (Recurrence after 5FU treatment)	Hepatocellular carcinoma (Recurrence & Metastasis after nexavar treatment)	Hepatocellular carcinoma (Recurrence & Metastasis after FOLFOX treatment)	Hepatocellular carcinoma (Recurrence & Metastasis after FOLFOX treatment)	Hepatocellular carcinoma (metastasis)	Hepatocellular carcinoma (metastasis)	Hepatocellular carcinoma (Recurrence & Metastasis after FOLFOX treatment)	Hepatocellular carcinoma (metastasis	Hepatocellular carcinoma (Recurrence & Metastasis after FOLFOX treatment	Hepatocellular carcinoma (Recurrence & Metastasis after cisplatin treatment)	Hepatocellular carcinoma (Recurrence & Metastasis after nexavar treatment)	Hepato cellular carcinoma (Metastasis after nexavar treatment
Classification of specimen used for culture	Fresh tumor	Fresh tumor	Fresh tumor	Fresh tumor	Fresh tumor	Fresh tumor	Fresh tumor	Fresh tumor	Fresh tumor	Fresh tumor	Fresh tumor	Fresh tumor	Fresh tumor	Fresh tumor
Obtained from	Severance Hospital, Seoul, Korea	Severance Hospital, Seoul, Korea	Severance Hospital, Seoul, Korea	Severance Hospital, Seoul, Korea	Severance Hospital, Seoul, Korea	Severance Hospital, Seoul, Korea	Severance Hospital, Seoul, Korea	Severance Hospital, Seoul, Korea	Severance Hospital, Seoul, Korea	Severance Hospital, Seoul, Korea	Severance Hospital, Seoul, Korea	Severance Hospital, Seoul, Korea	Severance Hospital, Seoul, Korea	Severance Hospital, Seoul, Korea

were randomly grouped (n = 10 per group). Tumor size was calculated with calipers, and tumor volume was measured using the following formula: $L \times S^2/2$ (where L and S are the longest and shortest diameters, respectively). After 13 days, When tumors attained a size of 100–200 mm^3, the tumor-bearing mice were randomly grouped and administered 40 mg/kg regorafenib (p.o.), 5 mg/kg cisplatin (p.o.), 80 mg/kg sorafenib (p.o.) alone or a combination of 20 mg/kg regorafenib (p.o.), 2.5 mg/kg cisplatin (p.o.), 40 mg/kg sorafenib (p.o.) with SERCA inhibitors 25 mg/kg (p.o.) (thapsigargin, candidate 56 or 62) once every other day. Different doses of candidate 56 or 62 were screened for dose selection. The doses of regorafenib, cisplatin and sorafenib was fixed every 20, 2.5 and 40 mg/kg. The tumor volume was quantified every two days using calipers. Animals were maintained under specific pathogen-free conditions. All experiments were approved by the Animal Experiment Committee of Yonsei University (IACUC approval No 2022–0105).

2.18. H&E (Hematoxylin and Eosin) and masson trichrome staining for establishment to hepatic and cardiac injury

Hepatic and cardiac biopsy specimens fixed in 10 % formalin solution were fitted with paraffin. Sections (5 μm) were stained with masson trichrome or H&E. The degree of cellular changes in hepatic and cardiac injury was evaluated with masson trichrome or H&E assay folowing manufacturer's protocols. The procedure stains nuclei dark red, muscle fibres and cytoplasm red, and ECM components blue.

2.19. Statistical analyses

Statistical analyses were conducted with GraphPad Prism (version 6.0; GraphPad Software, La Jolla, CA, USA), and immunohistochemistry results were assessed using analysis of deviation by Bonferroni post-hoc test. Values are indicated as the mean ± standard deviation, and $p < 0.05$ indicated statistical significance.

3. Results

3.1. Patients and disease characteristics

This study targeted and isolated cancer cell from speciment of cancer patients who took anti-cancer drugs but caused metastasis. The patient group consists of nine men and five women, a total of fourteen (Fig. 1A and Table 1). Compared to patient-derived non-metastatic (included Huh7) or metastatic HCC cells, metastatic HCC cells showed increase of metastatic markers (*NDUFA4L2, EBF1, TYMP [Thymidine phosphorylase] and MET*) (Fig. 1B), cancer stemness markers (*PROM1 [CD133], ALDH1A1, KRT17 and KRT19*) (Fig. 1C) and EMT markers (*SNAIL1 and 2, ZEB 1 and 2, WNT1 and 4, TWIST1*) (Fig. 1D) than non-metastatic HCC. Well-known HCC marker GPC-3 (glypican-3) and HCP70 (Heat shock protein 70) expression was compared normal liver cell (THLE-2) and established HCC cell line (Huh7, HepG2, Hep3B) in patient-derived HCC cells (Fig. 1E). Among the 14 patient, 3 patient-derived HCC cells were selected for current study. The patient cohort comprised four men (Table 1 and Fig. 2). Detailed characteristics of patient-derived hepatocellular carcinoma (HCC) and clinical features are provided in Table 1. The non metastatic HCC cell line, YUMC-NM-H1, was isolated from the postoperative specimen of a 71-year-old woman who was unexposed to preoperative chemotherapy or radiotherapy (Fig. 2A and E). Conversely, metastatic cell lines, YUMC-M−H1, YUMC-M−H2, and YUMC-M−H3, were isolated from specimens of three patients (53-year-old woman, 67 and 71-year-old man) with metastasis HCC at the time of surgery (Fig. 2B–D and F–H); among these, two patients had peritoneal and diaphragmatic metastases. The primary tumors at the time of surgery and preoperative radiologic findings are presented in Fig. 2. In the computed tomography (CT) findings, the yellow circle (Fig. 2A) indicates a primary mass without metastasis (Fig. 2E) and red circles (Fig. 2B–D) indicate metastatic HCC (Fig. 2F–H).

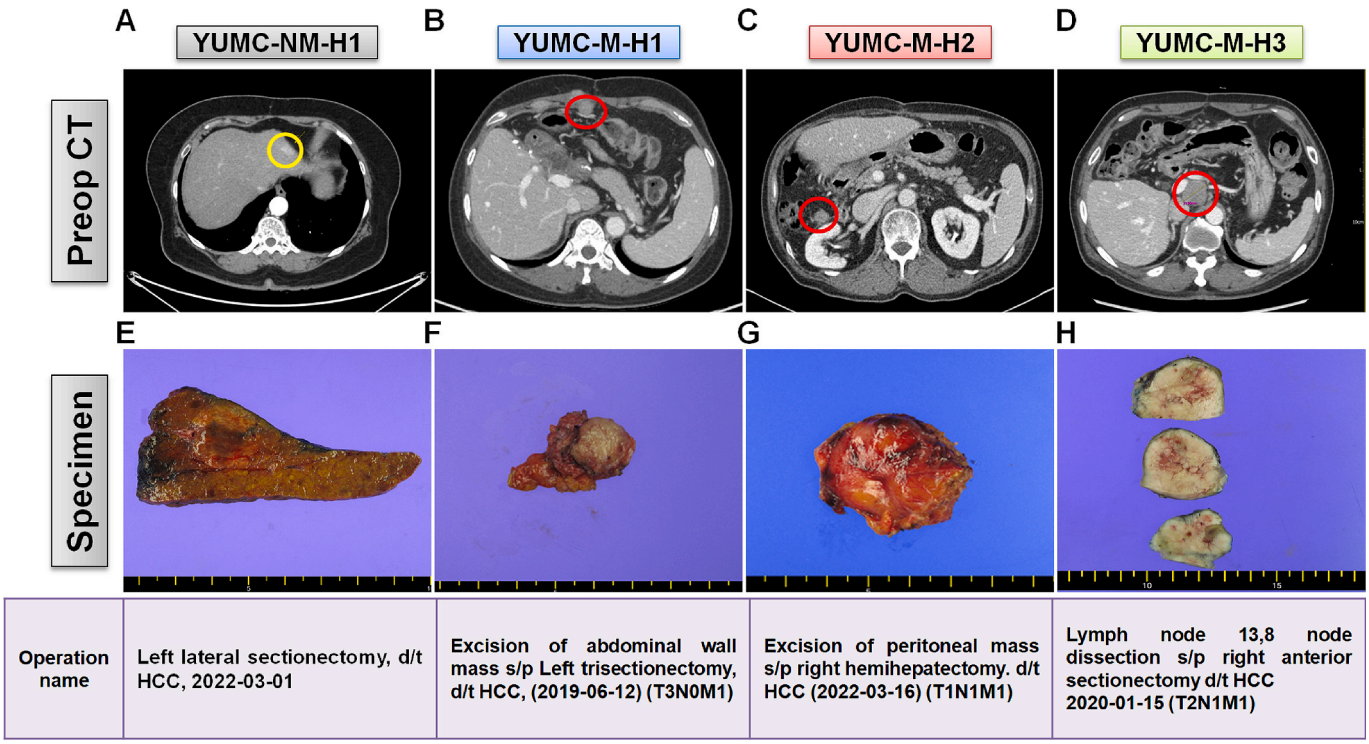

Fig. 2. Patient or specimen information for the patient-derived Hepatocellular carcinoma (HCC) cell line used in the study. A–D, computed tomography (CT) scan images. E–H, primary tumor figures of HCC patients. A and E, CT image and sectioned photo of the primary tumor of a 71-year-old woman diagnosed with HCC. The non-metastatic HCC cell line, YUMC-NM-H1, was isolated from this specimen. She presented with a 2.5 cm multinodular-confluent HCC located in segment 3 of the liver. B and F, CT image and sectioned photo of the primary tumor of a 53-year-old woman also diagnosed with HCC; the YUMC-M−H1 cell line was isolated from this specimen. C and G, CT image and sectioned photo of the primary tumor of a 67-year-old man diagnosed with HCC; the YUMC-M−H2 cell line was isolated from this specimen. D and H, CT image and sectioned photo of the primary tumor of a 71-year-old man diagnosed with HCC; the YUMC-M−H3 cell line was isolated from this specimen. Yellow circles show primary mass without metastasis and recurrence. Red circles indicate observed metastasis. (For interpretation of the references to colour in this figure legend, the reader is referred to the web version of this article.)

Table 2
Properties and clinical features of patients. Patient-derived Hepatocellular carcinoma cells were isolated from these patient specimen.

	YUMC-NM-H1	YUMC-M−H1	YUMC-M−H2	YUMC-M−H3
Age at Diagnosis	71	53	67	71
Gender	Female	Female	Male	Male
Primary Disease Site	Liver	Liver	Liver	Liver
Stage	T1bN0M0	T3N0M1	T1N1M1	T2N1M1
Primary Pathology	Hepatocellular carcinoma	Hepatocellular carcinoma (Metastasis after sorafenib treatment)	Hepatocellular carcinoma (Metastasis after sorafenib treatment)	Hepatocellular carcinoma (Metastasis after sorafenib treatment)
Classification of specimen used for culture	Fresh tumor	Fresh tumor	Fresh tumor	Fresh tumor
Obtained from	Severance Hospital, Seoul, Korea	Severance Hospital, Seoul, Korea	Severance Hospital, Seoul, Korea	Severance Hospital, Seoul, Korea

3.2. Differential gene expression and signal activation between non-metastatic and metastatic HCC cells in sorafenib treatment-induced acute ER stress conditions

Previously, we demonstrated that acute glucose deprivation or anti-cancer drug treatment increases metabolic stress, leading to favorable subclone classification with CSC properties [8,9]. Furthermore, under acute ER stress conditions, CSC-like properties and intensified induction of signaling pathways involved in survival are observed in some selectively surviving cells compared to those in their parental lineages [8,9]. To identify differences in gene expressions and signaling pathways between non-metastatic and metastatic HCC cells under anti-cancer drug-induced acute ER stress, we performed RNA sequencing-mediated transcriptome analysis. Current study, we used the patient-derived HCC cells, YUMC-NM-H1 (non-metastatic HCC) and YUMC-M−H1, –H2, and –H3 (metastatic HCC). Four tissue samples (patients were treated at the Severance Hospital, Yonsei University College of Medicine, Seoul, Korea) were obtained from two patients with divergent HCC properties (Table 2, HCC in non-metastatic HCC was termed "YUMC-NM-H1" and that in metastatic as "YUMC-M−H1, –H2, and –H3"). Considering that gene expression is primarily dependent on metastasis, we hypothesized that metastasis involves an advanced cancer phenotype induced by epigenetic reprogramming, relative to that in non metastatic HCC cells. Therefore, metastatic HCC cell survival may involve epigenetic gene pathway induction which regulates calcium (for overburdened cytosolic free calcium regulation), peroxisome proliferator-activated receptors (PPAR; for mitochondrial metabolism), nuclear factor kappa B (NFκB; for metabolic adaptation or energy homeostasis), and Notch and Wnt signaling pathways under anti-cancer drug-treated acute ER stress conditions. NFκB is an anti-apoptotic factor known for its

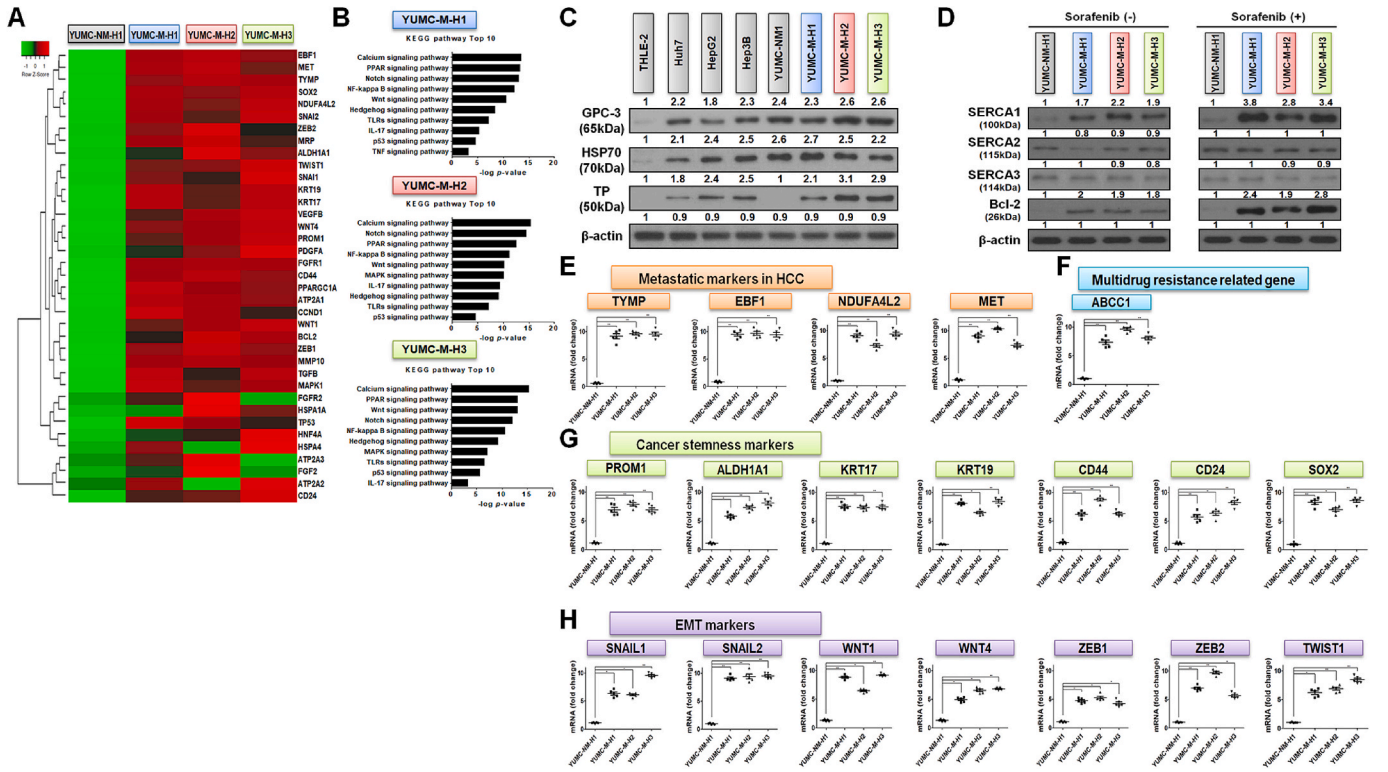

Fig. 3. Signaling pathway and target gene expression profiling in patient-derived HCC cells under basal or sorafenib-mediated endoplasmic reticulum (ER) stress conditions. A, Hierarchical clustering shows differential gene expression; gene expression profiles in the metastatic HCC cells compared to those in patient-derived non-metastatic HCC cells. B, Bar plot revealed 10 prominently stimulated pathways in the patient-derived metastatic HCC cells compared to those in patient-derived non-metastatic HCC cells. C, Immunoblot analysis for validation of HCC or metastatic marker expressions between the non-metastatic and metastatic HCC cells compare than normal liver cell. D, Alterations of the target genes through immunoblot assay under basal or sorafenib-mediated sever ER stress condition between non-metastatic and metastatic HCC cells. E–H, Gene expression variances were evaluated on mRNA sequencing (mRNA seq) analysis between the non-metastatic and metastatic HCC cells. E, Each assay was performed at least in triplicate. *$p < 0.05$ and **$p < 0.01$ versus non-metastatic HCC, YUMC-NM-H1.

transcriptional role in SERCA expression [9]. Moreover, NFκB is a pivotal regulator of mitochondrial respiration, metabolic adaptation, and energy homeostasis [27]. Compared to non-metastatic HCC cells (YUMC-NM-H1), metastatic markers (*TYMP [Thymidine phosphorylase], EBF1 [early B cell factor 1], NDUFA4L2 [NADH dehydrogenase (ubiquinone) 1 alpha subcomplex 4-like 2], and MET [Mesenchymal epithelial transition factor]*), multidrug resistance related gene (ABCC1 [MRP]), cancer stemness markers (*PROM1 [CD133], ALDH1A1, KRT17, KRT19, CD44, CD24 and SOX2*) and EMT markers (*SNAIL1, SNAIL2, WNT1 WNT4, ZEB1[Zinc finger E-box-binding homeobox1], ZEB2 and TWIST1 [twist family bHLH transcription factor1]*) were significantly increased in metastatic HCC cells, YUMC-M−H1, –H2 and –H3 (Fig. 3A and 1E–H). In metastatic HCC, we concentrated on highly ranked gene modules involved in survival-related signaling pathways, including Notch, calcium, Hedgehog, and Wnt (Fig. 3B), particularly calcium signaling pathways which were overstimulated in metastatic HCC cells. Well-known HCC marker (GPC-3 and HCP70) and metastatic marker (TP; Thymidine phosphorylase) expression was compared normal liver cell (THLE-2) and established HCC cell line (Huh7, HepG2, Hep3B) in patient-derived HCC cells (Fig. 3C). Basal level of HCC and metastatic marker expressions were significantly increased in established HCC and patient-derived metastatic HCC than normal liver cell (Fig. 3C). Basal SERCA1 and anti-apoptosis marker Bcl-2 (B cell lymphoma-2) levels (critical components involved in anti-apoptosis and calcium homeostasis) [28] were significantly higher in metastatic HCC cells than in non-metastatic HCC cells. On treatment with anti-cancer drugs such as sorafenib, SERCA1 and Bcl-2 expression notably increased in metastatic HCC cells compared to those in non-metastatic HCC cells (Fig. 3D). SERCA2 and SERCA3 expression showed no significant differences between the two HCC cells, regardless of sorafenib treatment (Fig. 3D).

In summary, the calcium regulation signaling pathway or survival-related gene simulation in managing calcium regulation and SERCA are pivotal factors for survival under anti-cancer drug, sorafenib-induced metabolic stress conditions in metastatic HCC cells.

3.3. Metastatic HCC cell survival during prolonged anti-cancer drug treatment-stimulated metabolic stress depends on increased CaMK2α-mediated SERCA1 expression

Excessive cytosolic free calcium is primarily involved in cell death [29]. Calcium channels, exchangers, and pumps are managed by a cytosolic-free calcium overburden and are pivotal regulators of cellular fate in physiological and pathological microenvironments [12,29]. CaMK2α is a known as factor to increase in the nuclear translocation of NFκB which regulates of Bcl-2, SERCA and PGC1α [10,28,30]. We initially determined alterations in pCaMK2α, pIKKα (I kappa B kinase), Bcl-2 (anti-apoptotic marker), SERCA1, CHOP (*C/EBP homologous protein*, ER stress marker), cleaved-caspase3 (apoptotic marker), nuclear located NFκB in the presence or absence of anti-cancer drug (sorafenib) in non-metastatic (YUMC-NM-H1) and metastatic (YUMC-M−H1, –H2 and –H3) HCC (Fig. 4A). Under anti-cancer drug treatment-mediated acute ER stress conditions, metastatic HCC was evaded ER stress (CHOP) or apoptosis (cleaved-caspase3) via increase of nuclear located NFκB, Bcl-2 and SERCA1 by CaMK2α (Fig. 4A). Based on results of electrophoretic mobility shift aasy (EMSA), enhancement the nuclear translocation of NFκB (Fig. 5A–C) by stimulating CaMK2α (pCaMK2α, phosphorylated CaMK2α), which subsequently upregulated the transcription of SERCA1 and Bcl-2 in metastatic HCC cells compared to that in non-metastatic HCC cells (Fig. 4A and Fig. 5A–C). Consequently, we evaluated the causal relationship between elevated SERCA1 levels and

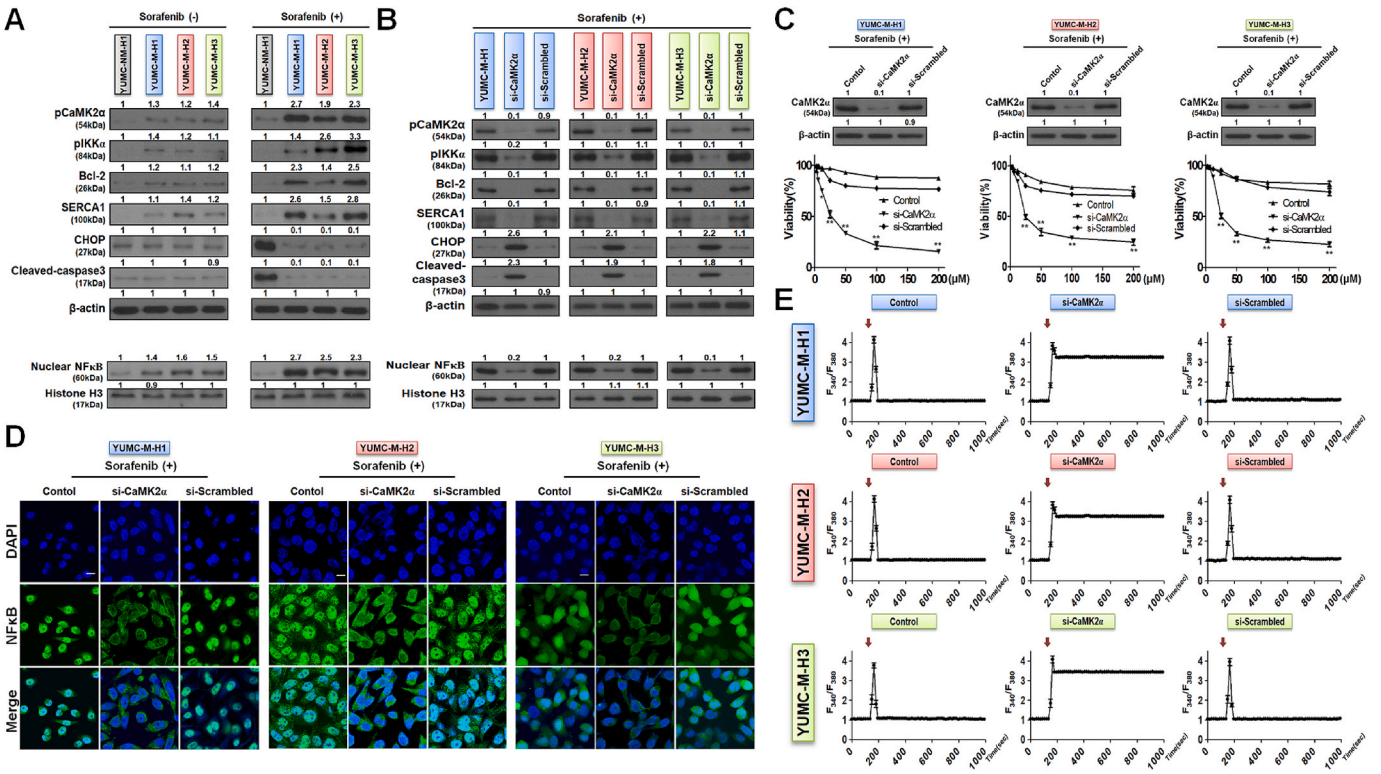

Fig. 4. Patient-derived metastatic HCC cell survival was prolonged through the nuclear translocation of nuclear factor kappa B (NFκB) by calcium/calmodulin-dependent protein kinase alpha (CaMK2α), which mediated an increase in SERCA1 levels under sorafenib-treated conditions. A, Immunoblot analysis revealed that the regulation of nuclear translocation of nuclear factor kappa B (NFκB) by CaMK2α influenced proteins related to calcium restoration (SERCA1), ER stress (CHOP), apoptosis (cleaved caspase 3), and anti-apoptosis (Bcl-2) under the presence or absence of sorafenib between non-metastatic and metastatic HCC cells. B and C, Immunoblot analysis (B) and cell viability assay (C) of CaMK2α-silenced metastatic HCC cells, YUMC-M−H1, –H2, and –H3 on treatment with sorafenib (left; YUMC-M−H1, middle; YUMC-M−H2, right; YUMC-M−H3). *$p < 0.05$ and **$p < 0.01$ versus control (unmodified metastatic HCC cells, YUMC-M−H1, –H2, and –H3 under sorafenib treatment). D, Immunofluorescence assay for nuclear expression of NFκB in CaMK2α-silenced metastatic HCC cells under sorafenib-treated conditions. Magnification, × 400. Scale bar, 20 μm. Data represent the average of at least three separate independent experiments and are presented as the means ± SEM. E, Cytosolic free calcium content in CaMK2α-silenced metastatic HCC cells, YUMC-M−H1, –H2, and –H3 under sorafeni treatment. The red arrow shows the high potassium depolarization which induces an increase in cytosolic calcium. Each assay was performed at least in triplicate. (For interpretation of the references to colour in this figure legend, the reader is referred to the web version of this article.)

CaMK2α by CaMK2α knockdown in metastatic HCC (YUMC-M−H1, –H2, and –H3 small interfering [si]-*CaMK2α*) with sorafenib (Fig. 4B–E). Immunoblot analysis (Fig. 4B) and cell viability assay (Fig. 4C) indicated that *CaMK2α* knockdown in metastatic HCC cells using siRNAs downregulated cell viability and decrease of pIKKα, Bcl-2 and SERCA1 levels through inhibition of nuclear translocated NFκB under sorafenib treatment conditions (Fig. 4B–C). Consequently, *CaMK2α* knockdown in metastatic HCC cells significantly increased the levels of apoptotic markers CHOP and cleaved caspase 3, while considerably decreasing those of pCaMK2α, pIKKα, Bcl-2, SERCA1, and nuclear translocated NFκB under acute ER stress conditions by sorafenib treatment (Fig. 4B). Viability assays showed the dose-dependent restriction of prolonged survival with sorafenib in downregulated CaMK2α metastatic HCC cells (Fig. 4C, left; YUMC-M−H1, middle; YUMC-M−H2, right; YUMC-M−H3). Immunofluorescence assays of *CaMK2α* knockdown in metastatic HCC cells showed that the nuclear translocation of NFκB was considerably inhibited by *CaMK2α* knockdown (Fig. 4D). Microspectrofluorimetry revealed that the *CaMK2α* knockdown-mediated inhibition of SERCA1 and Bcl-2 influenced intracellular calcium levels in metastatic HCC cells following sorafenib treatment (Fig. 4E). Cytosolic free calcium levels were measured in response to high potassium depolarization, which triggered an increase in the levels of cytosolic free calcium; its clearance was estimated in the presence or absence of sorafenib based on separate calcium fluxes. Cytosolic free calcium levels were restored to the basal levels in the control and si-scrambled group after sorafenib each treatment in metastatic HCC cells (Fig. 4F, top; YUMC-M−H1, middle; YUMC-M−H2 and bottom; YUMC-M−H3). However, this restoration was interrupted by CaMK2α knockdown via si-*CaMK2α* in metastatic HCC cells.

In summary, metastatic HCC cells can ameliorate calcium-mediated apoptosis under anti-cancer drug treatment by increasing SERCA1 levels through inducing nuclear NFκB translocation via CaMK2α, which is a pivotal transcriptional contributor to SERCA1 and Bcl-2 upregulation.

3.4. Candidate 56 and 62 identification as SERCA1 target-specific inhibitors using molecular docking simulation and structure modeling

We hypothesized and demonstrated that metastatic HCC cells and functional SERCA1 inhibition would be a practical clinical strategy for patients with metastatic HCC. We identified novel, small SERCA1-specific binding molecules as well as the possibility of pharmacophore-binding modes. Consequently, we identified two novel small molecules, candidate 56 and 62, which showed pharmacophoric high SERCA1-specific binding affinity, resulting in critical functional suppression of SERCA1. An evolutionary chemical binding similarity (ECBS) program was used to elucidate the inhibitory mechanisms of candidate 56 and 62 (Fig. 6A–C). ECBS analysis using a categorization affinity learning framework defined with paired target's evolutionary relationship and chemical data. The ECBS method is invented to encode molecular properties enriched in evolutionarily preserved chemical-target binding correlations, and formulated by the probability of chemical compounds associating to identical targets [31]. To recognize

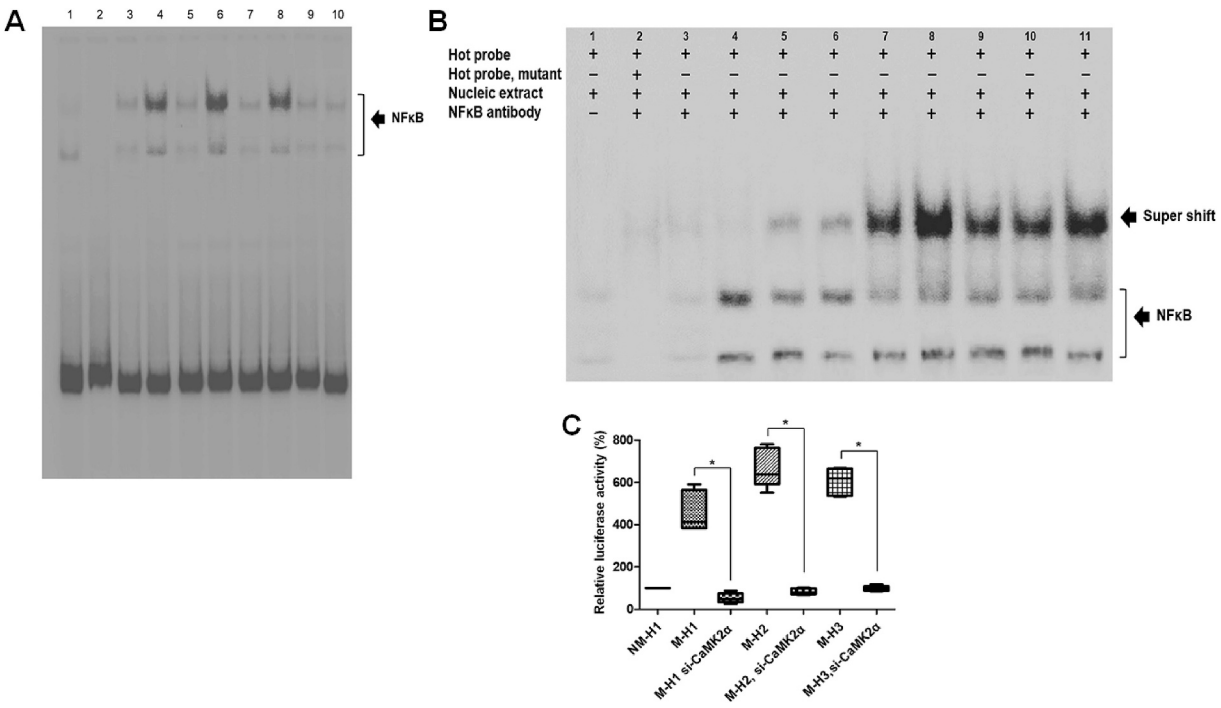

Fig. 5. Metastatic HCC survival during prolonged sorafenib treatment–induced metabolic stress depended on SERCA1 expression induction by CaMK2α-mediated nuclear translocated NFκB. A, EMSA assay of NFκB, its transcriptional factor NFκB with the SERCA1 promoters. Lane 1; Control (NFκB hot probe) + YUMC-NM-H1, nucleic extract, lane 2; Mutant (NFκB hot probe, mutant) + YUMC-NM-H1, nucleic extract, lane 3; YUMC-M−H1, si-CaMK2α (NFκB hot probe + nucleic extract), lane 4; YUMC-M−H1 (NFκB hot probe + nucleic extract), lane 5; YUMC-M−H2, si-CaMK2α (NFκB hot probe + nucleic extract), lane 6; YUMC-M−H2 (NFκB hot probe + nucleic extract), lane 7; YUMC-M−H3, si-CaMK2α (NFκB hot probe + nucleic extract), lane 8; YUMC-M−H3 (NFκB hot probe + nucleic extract), lane 9; YUMC-NM-H1, si-CaMK2α (NFκB hot probe + nucleic extract), lane 10; YUMC-NM-H1 (NFκB hot probe + nucleic extract), B, Lane 1; Control (NFκB hot probe) + YUMC-NM-H1 nucleic extract, lane 2; Mutant (NFκB hot probe, mutant) + YUMC-NM-H1 nucleic extract + NFκB antibody 3ug, lane 3; YUMC-NM-H1, NFκB hot probe + nucleic extract + NFκB antibody 3ug), lane 4; YUMC-M−H1,si-CaMK2α (NFκB hot probe + nucleic extract + NFκB antibody 3ug), lane 5; YUMC-M−H2,si-CaMK2α (NFκB hot probe + nucleic extract + NFκB antibody 3ug), lane 6; YUMC-M−H3,si-CaMK2α (NFκB hot probe + nucleic extract + NFκB antibody 3ug), lane 7; YUMC-M−H1 (NFκB hot probe + nucleic extract + NFκB antibody 3ug), lane 8; YUMC-M−H2 (NFκB hot probe + nucleic extract + NFκB antibody 3ug), lane 9; YUMC-M−H3 (NFκB hot probe + nucleic extract + NFκB antibody 3ug), lane 10; YUMC-M−H1 (NFκB hot probe + nucleic extract + NFκB antibody 1ug), lane 11; YUMC-M−H2 (NFκB hot probe + nucleic extract + NFκB antibody 1ug), C, Dual Luciferase Reporter Assay, which was used to compare NFκB transcriptional activity between non-metastatic and metastatic HCC in CaMK2α knockdown. **P < 0.01 vs non-metastatic HCC cell, YUMC-NM-H1.

the molecular interactions of candidate 56 and 62, we carried out blind docking simulations, followed by local docking refinement and energy minimization. A blind docking simulation was performed using the human SERCA1 structural model to predict the ligand-binding site and molecular interactions (Fig. 6D and G). A similarity search using FoldSeek [32] server revealed that the structure of human SERCA1 is highly similar to that of rabbit SERCA1 (PDB ID 6YSO, UniProt ID P04191), with a sequence identity of 95.3 % and root mean square deviation of 1.89 Å (TM-Score 0.971), indicating significant consistency between them. Docking complex models suggested the potential binding of candidate 56 and 62 to the cavity between the n and p domains in the cytoplasmic region of SERCA1, overlapping with the binding site of the ATP derivative (PubChem CID 644358) found in the rabbit SERCA1 structure [33]. The docking scores, obtained through all-atom minimization with Rosetta, were −14.3 and −13.4 (in Rosetta Energy Unit) for candidate 56 and 62, respectively. Despite their similar binding scores and chemical structures, candidate 56 and 62 exhibited contrasting binding orientations in the docking models, presumably due to their distinct 3D conformations (Fig. 6E and F). In candidate 56, the aromatic ring with a chlorine atom was directed towards F487 and M494; whereas in candidate 62, it interacted with P518 (Fig. 6E and F). Notably, F487 consistently participated in pi-pi interactions with the aromatic rings of both compounds. Additionally, R560 showed a polar interaction only with candidate 62, presumably contributing to its binding specificity, along with additional interactions with L562 and T441. In contrast, A517 and K492 cells exhibited more hydrophobic interactions with candidate 56. Pharmacophore models based on the receptor–ligand interactions are constructed to highlight the essential interactions within the ligands (Fig. 6H). These ligand–protein interactions observed in the docking models have the potential to offer valuable observations into the molecular basis of their activity, aiding efficient molecule design in the future.

These protein–ligand interactions, as suggested by the docking models, have the potential to elucidate the molecular basis of the ligand activity. However, experimental validation is still necessary in future studies.

3.5. Candidate 56 and 62 increase of restraint the survival of metastatic HCC cells through failed to revert to basal levels after cytosolic free calcium spike

We conducted cell viability assays to examine the anti-cancer impact of the novel small molecules and SERCA1-specific inhibitors, candidate 56 and 62. The results showed that non-metastatic HCC cells exhibited considerably reduced viability in a dose-dependent manner after sorafenib treatment, regardless of whether it was used in conjunction with SERCA inhibitors (Fig. 7A). Treatment with candidate 56 or 62 alone had a marginal anti-cancer influence on non-metastatic HCC cells (Fig. 7A). Moreover, the viability of metastatic HCC cells was not significantly affected by the SERCA inhibitors or sorafenib treatment alone. In contrast, novel SERCA1-specific inhibitor candidate 56 and 62 used in combination with sorafenib remarkably reduced metastatic HCC cell viability in a dose-dependent manner (Fig. 7B–D). SERCA is a fundamental player and therapeutic target in the adjustment of cytosolic

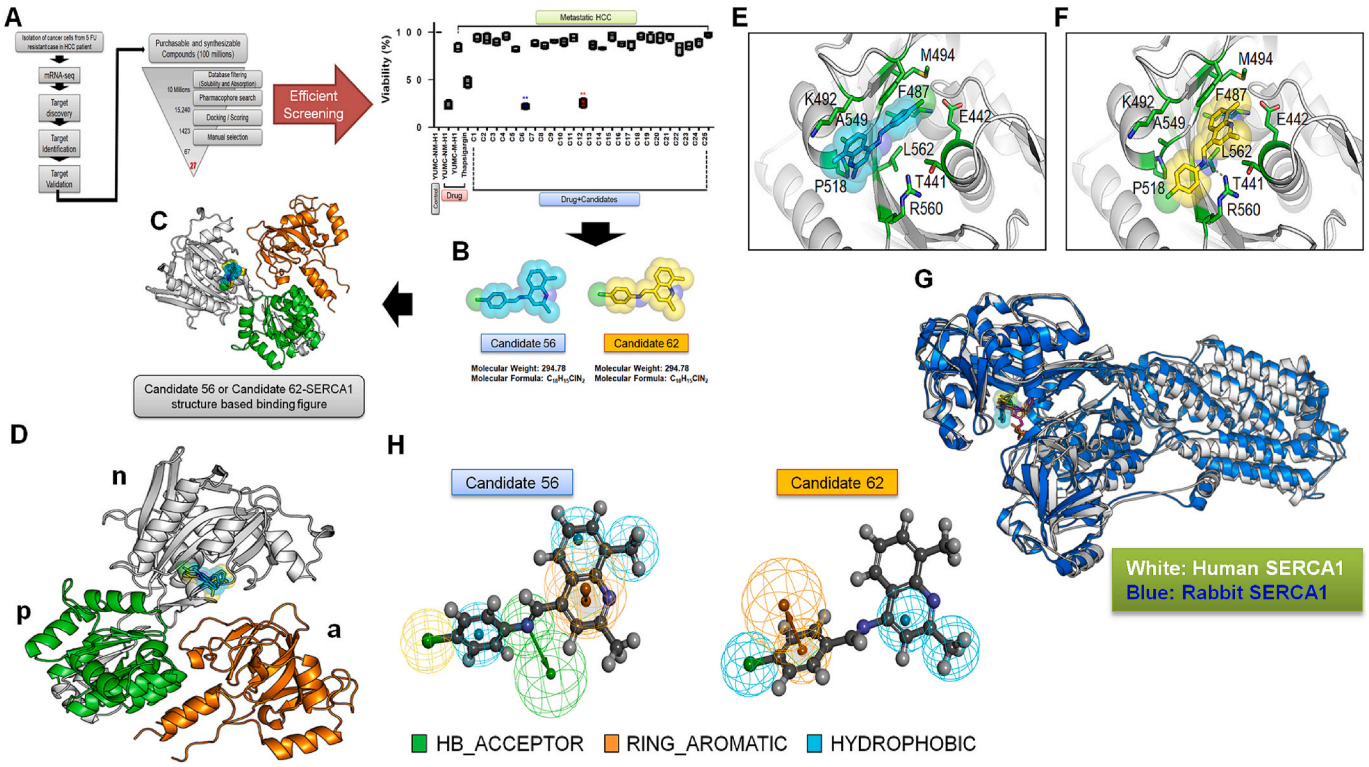

Fig. 6. Screening and molecular docking models of candidate 56 and 62 for SERCA1. A, Screening models for identification of candidate 56 and 62 in patient-derived metastatic HCC cells. B, The candidate 56 and 62 carbons are represented by cyan and yellow, respectively. C, The docking sites for candidate 56 and 62 in the cytosolic N domain of SERCA1. D, The N, P, and A domains are annotated and the binding residues are shown in blue. E and F, candidate 56 or 62 binding residues in SERCA1 are represented as sticks in green. The transmembrane regions are represented by a grey ribbon. The enlarged representation of protein–ligand interactions in the docking models highlight the binding residues involved in interactions with candidate 56 and 62. The pi-pi stacking of the compounds with F487 is indicated by a dotted yellow line. The different colors used in the Fig. correspond to the properties of the binding site residues. G, The alignment of (predicted) human SERCA1 and (X-ray crystal) rabbit SERCA1 structures are represented by cartoons (root mean square deviation of 1.89 Å). The human SERCA1 structure is shown in white, whereas the rabbit SERCA1 structure is shown in blue. The ATP-derivative bound to the rabbit SERCA1 structure (PDB ID 6YSO) is illustrated with red sti4Hcks, alongside the docking conformations of candidate 56 and 62 shown in cyan and yellow, respectively. H, Pharmacophore models based on the receptor–ligand interactions. (For interpretation of the references to colour in this figure legend, the reader is referred to the web version of this article.)

calcium overburden in cancer [15,34]. The anti-cancer effect of candidate 56 and 62 via the specific functional inhibition of SERCA1 was determined using microspectrofluorometry based on the differences in intracellular calcium levels in patient-derived non-metastatic and metastatic HCC cells medicated with sorafenib solitary or with SERCA inhibitors (Fig. 7E–H). Free cytosolic calcium levels were measured in the presence of high-potassium depolarization and were estimated solitary or combined sorafenib treatment with SERCA inhibitors (Thapsigargin; positive control, candidate 56, and candidate 62). Cytosolic free calcium levels in non-metastatic HCC cells failed to revert to basal levels following sorafenib treatment, regardless of whether it was used in conjunction with SERCA inhibitors (Fig. 7E). Sorafenib treatment alone in metastatic HCC cells, the cytosolic free calcium levels revert to the basal levels. However, when SERCA1-specific inhibitors candidate 56 and 62 were combined with each, cytosolic free calcium failed to revert to basal levels (Fig. 7F–H). There were no considerable changes in the levels of cytosolic free calcium on treatment with sorafenib or SERCA inhibitors alone in metastatic HCC cells.

These variations in cytosolic free calcium levels between patient-derived non-metastatic and metastatic HCC cells may be directly related to SERCA. To assess whether the prolonged survival of metastatic HCC cells on sorafenib treatment was indeed associated with only SERCA1 and not sodium-calcium exchangers (NCX), not calcium ion channels, not plasma membrane calcium ATPase (PMCA) we performed cell viability (Fig. 8A–D) and immunoblot assays (Fig. 8E) on treatment with NCX inhibitor (KB-R7943), calcium channel blockers (bepridil, verapamil or nifedipine), plasma membrane calcium PMCA inhibitor (caloxin2a1), and SERCA inhibitors in combination with sorafenib in non-metastatic and metastatic HCC cells (Fig. 8A–E). In non-metastatic HCC cells, no significant changes were observed on treatment with either agent with sorafenib compared to that with sorafenib treatment alone (Fig. 8A). In metastatic HCC cells, sorafenib treatment alone or combination treatment with NCX inhibitor, calcium channel blockers, PMCA inhibitor did not significantly influence survival, whereas combination treatment with SERCA inhibitors were failed to survive dose-dependently (Fig. 8B, C, and D). Results of the immunoblot assay indicated that CHOP (an ER stress marker) levels increased significantly on combining SERCA inhibitors and sorafenib treatment in metastatic HCC cells (Fig. 8E, top; right, bottom; left and right). However, in non-metastatic HCC cells, CHOP levels significantly increased in the presence of sorafenib regardless of treatment with an NCX inhibitor, calcium channel blocker, SERCA inhibitor, or PMCA inhibitor (Fig. 8E, top; left). To verify the role of candidate 56 and 62 as SERCA1-specific inhibitors, we assessed the anti-cancer effects of candidate 56 or 62 when used in combination with each anti-cancer drug (sorafenib, 5-Fluorouracil [5-FU] and gemcitabine) in other metastatic HCC cells (YUMC-M−H8; patient-derived HCC cells were isolated from metastatic tissue of a patient after 5FU therapy, YUMC-M−H12; patient-derived HCC cells were isolated from metastatic tissue of a patient after gemcitabine therapy) (Fig. 8F-I). mRNA quantification of metastatic HCC cells compare to non-metastatic HCC cells under each anti-cancer drug treated conditions showed increase in SERCA1 levels predominantly in YUMC-M−H1, –H2, and –H3; however, YUMC-M−H8 and YUMC-M−H12 showed significantly increased levels of the SERCA2 or SERCA3 isoforms respectively

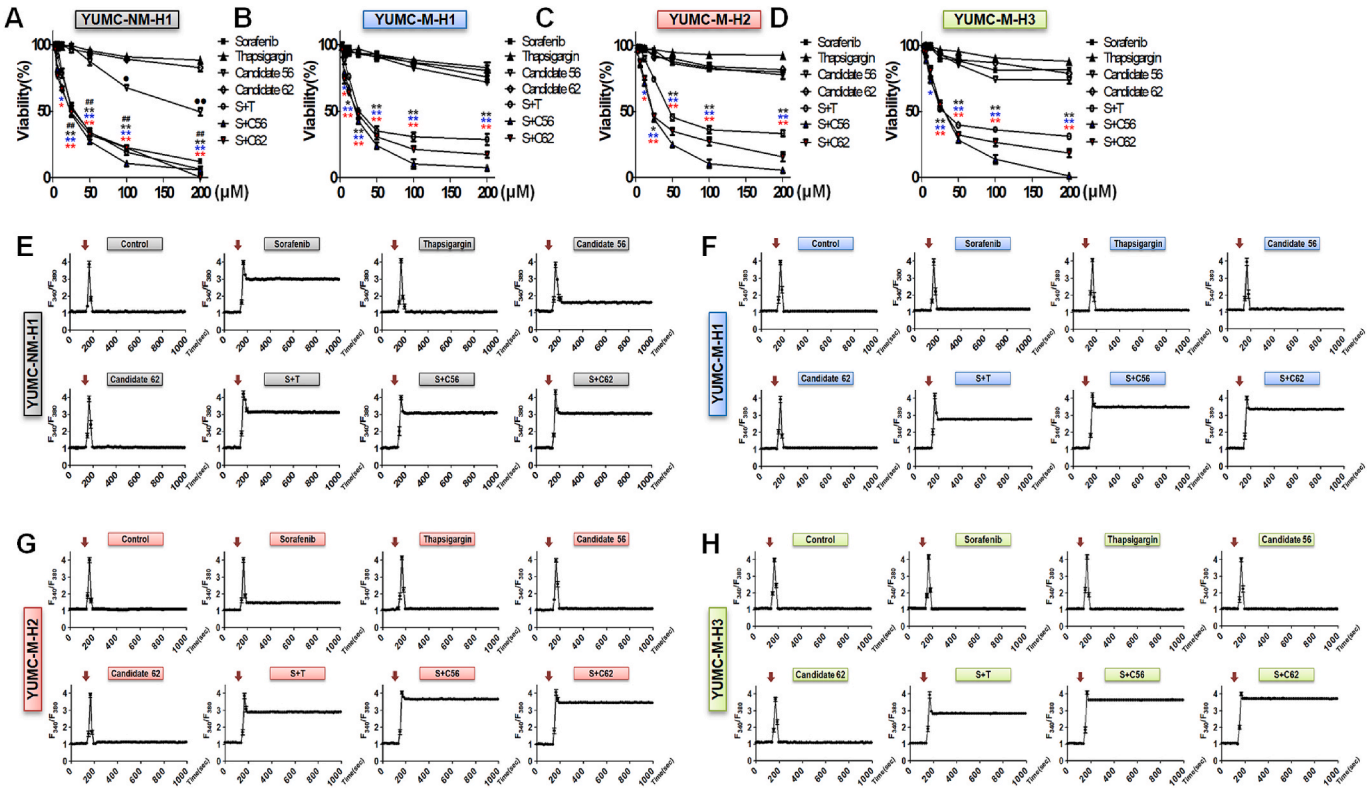

Fig. 7. Cell viability and cytosolic free calcium measurement in whole patient-derived HCC cells after thapsigargin (SERCA inhibitor, positive control) and molecular docking models of candidate 56 and 62 for SERCA1. A, The candidate 56 and 62 carbons are represented by cyan and yellow, respectively. B, The docking sites for candidate 56 and 62 in the cytosolic N domain of SERCA1. C–F, Cell viability assay between non-metastatic and −metastatic HCC cells on treatment with sorafenib and SERCA inhibitors alone or combination, excluding combination with SERCA inhibitors. G–J, Cytosolic free calcium measurement between non-metastatic and metastatic HCC cells on treatment with sorafenib and SERCA inhibitors alone or combination, excluding combination with SERCA inhibitors. The red arrow shows high potassium depolarization addition to increase cytosolic calcium. G, non-metastatic HCC cells, YUMC-NM-H1. H–J, metastatic HCC cells, YUMC-M−H1, −H7, and −H8. *p < 0.05 and **p < 0.01 versus control, *,**; thapsigargin, *,**; candidate 56, *,**; candidate 62. T; thapsigargin, S; sorafenib, C56; candiate 56, C62; candidate 62. Each assay was performed at least in triplicate. (For interpretation of the references to colour in this figure legend, the reader is referred to the web version of this article.)

(Fig. 8F). Protein quantification at the basal or anti-cancer drug (sorafenib, 5-FU and gemcitabine)-treated conditions using immunoblot assay further proved that the metastatic HCC cells, YUMC-M−H1, –H2, and –H3 significantly expressed SERCA1, whereas other metastatic HCC cells, YUMC-M−H8 and −H12 (patient-derived HCC cells, metastasis ocurred after 5-FU or gemcitabine therapy) significantly increased the SERCA2 and SERCA3 isoforms, respectively under anti-cancer drug treated conditions (Fig. 8G). ER stress marker, CHOP levels were not significantly different in metastatic HCC cells regardless of the anti-cancer drug used. However, non-metastatic HCC cells showed significantly increased CHOP levels on sorafenib treatment (Fig. 8G). In cell viability assays, combination treatment with the novel SERCA1 isoform-specific inhibitors (candidate 56 and 62) and anti-cancer drugs (sorafenib, 5-FU and gemcitabine), resulted in dominantly expressed SERCA1 (YUMC-M−H1, –H2, and –H3), SERCA2 (YUMC-M−H8), and SERCA3 (YUMC-M−H12), respectively, in the metastatic HCC cell line. Consequently, cell viability of SERCA1 dominantly expressed metastatic HCC cells was suppressed by SERCA1 isoform-specific inhibitors (candidate 56 and 62) with anti-cancer drug (Fig. 8H, left), whereas SERCA2 or SERCA3 dominantly expressed HCC was no significantly influenced candidate 56 and 62 with anti-cancer drug (Fig. 8H, right). Cell viability significantly decreased whereas CHOP levels increased in non-metastatic HCC cells on sorafenib treatment (Fig. 8I). However, metastatic HCC cells (YUMC-M−H1, –H2, –H3, −H8, and −H12) did not significantly influence cell viability or ER stress under anti-cancer drug (sorafenib, 5-FU and gemcitabine) alone treated conditions. These cells showed significantly decreased cell viability and increased CHOP levels following treatment with the SERCA1 isoform-specific inhibitors, candidate 56 and 62 (Fig. 8I). However, in SERCA2 and SERCA3 dominantly expressed HCC cells, YUMC-M−H8 and −H12, respectively, showed no significant difference in cell viability and increase in ER stress on combined treatment with anti-cancer drugs (5FU or gemcitabine) and candidate 56 or 62. Therefore, the novel SERCA inhibitors candidate 56 and 62 could be considered as SERCA1-specific inhibitors.

These findings imply that SERCA1 regulates survival prolongation in metastatic HCC cells during chemotherapy treatment by mediating overloaded cytosolic free calcium levels through new SERCA1 isoform-specific inhibitors, candidate 56 and 62.

3.6. A novel therapeutic approach for metastatic HCC through SERCA1-specific inhibitors (novel small molecules, candidate 56 and 62) in a patient-derived metastatic HCC cell mouse xenograft model

We evaluated the anti-cancer effects of candidate 56 and 62 *in vivo* using a mouse xenograft tumor model with SERCA1, which predominantly increased patient-derived metastatic cells. We induced acute ER stress by treatment with sorafenib alone or with SERCA inhibitors. The dose of candidate 56 and 62 in xenograft model was selected in a dose-dependent manner following candidate 56 and 62 treatment with sorafenib (Fig. 9A–C). In the xenograft model with non-metastatic HCC cells, conspicuous tumor shrinkage increased due to sorafenib treatment regardless of SERCA inhibitor combination treatment (Fig. 10A, top). In the metastatic HCC xenograft model, sorafenib treatment alone did not increase tumor shrinkage; however, combinatorial treatment with

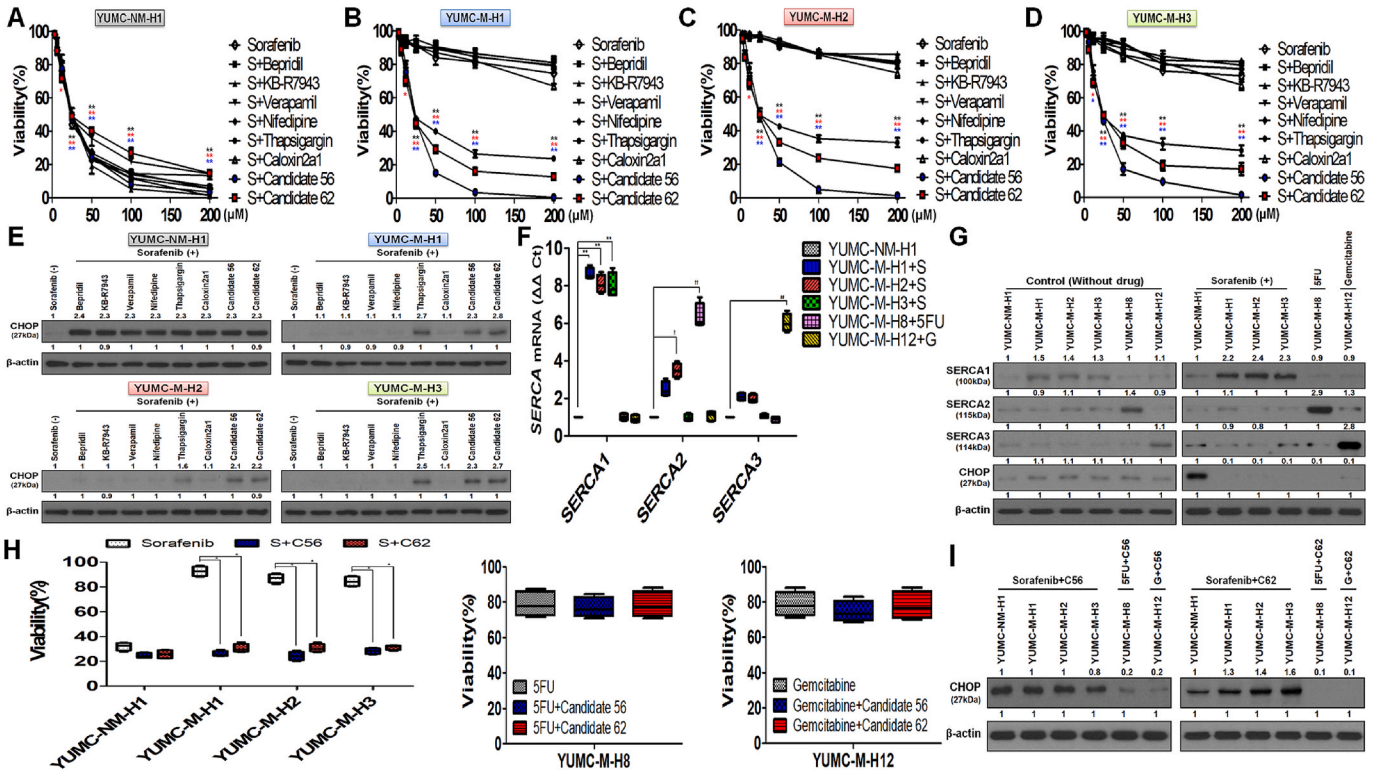

Fig. 8. Cell viability assay in whole patient-derived HCC cells after treatment with SERCA1 isoform specific novel candidate (candidate 56 and 62) treatment in the presence of anti-cancer drug (sorafenib, 5FU and gemcitabine). A–D, Dose-dependent cell viability in the presence of calcium channel blocker (bepridil, verapamil, or nifedipine), sodium-calcium exchangers (NCX) inhibitor (KB-R7943), plasma membrane calcium ATPase (PMCA) inhibitor (caloxin 2a1), and SERCA inhibitors (thapsigargin, candidate 56 and 62) with sorafenib between non-metastatic and −metastatic HCC cells. *p < 0.05 and **p < 0.01 versus control (the absence of sorafenib), **; thapsigargin, *,**; candidate 56, *,**; candidate 62, S; sorafenib. E, Immunoblot analysis for ER stress marker induction under combination treatment with the various inhibitors and sorafenib between non-metastatic and metastatic HCC cells. F, Differential SERCA isoform-dependent RNA expression in the metastatic (YUMC-M−H1, –H2, and –H3), 5FU-resistant-mediated metastatic HCC (YUMC-M−H8), and gemcitabine-resistant mediated (YUMC-M−H12) cells compared to those in non-metastatic HCC cells. S; sorafenib, G; gemcitabine. *p < 0.05 and ** p < 0.01 versus non-metastatic HCC cells. G, Immunoblot analysis for the differential dominance of SERCA isoforms-mediated induction of ER stress marker between non-metastatic and metastatic (sorafenib, 5FU or gemcitabine-resistant mediated HCC) cells under each agent presence or absence conditions. H and I, Cell viability (H) and immunoblot assay (I) for the selective suppression of viability or selectively inducing ER stress under combination treatment of candidate 56 or 62 with sorafenib, 5FU or gemcitabine in non-metastatic and metastatic (sorafenib, 5FU or gemcitabine-resistant mediated HCC) HCC cells. S; sorafenib, C56; candidate 56, C62; candidate 62, G; gemcitabine. *p < 0.05 versus control (sorafenib only treatment). Each assay was performed at least in triplicate.

sorafenib and candidate 56 or 62, novel SERCA1 isoform-specific inhibitors resulted in remarkable tumor shrinkage (Fig. 10B–D, top). The excised tumors were similar in terms of tumor volume, which declined considerably with sorafenib treatment, regardless of the presence of SERCA inhibitors in the non-metastatic HCC cells (Fig. 10A, middle). By comparison, dissected tumor weight in metastatic HCC cells was not meaningful influenced by each sorafenib alone, whereas combinatorial strategy to sorafenib with candidate 56 or 62 leaded a prominent decrease in tumor weight (Fig. 10B–D, middle). All the inhibitory agents, administered alone or in combination, did not significantly influence the whole body weight of mice (Fig. 10A–D, bottom). Further, morein the change of survival rate (Fig. 6E) and whole body weight (Fig. 9D) were measured under treatment with thapsigargin, candidate 56, or 62 alone in normal mice (not xenograft model) and compared with a non-treated group for 29 days. In normal mice, candidate 56 or 62 treatment alone showed no significant difference in whole body weight or death ratio compared with the group treated with thapsigargin alone (Fig. 10E and Fig. 9D). Tumor lysate-based immunoblot assay of non-metastatic HCC cells revealed that SERCA1 expression did not significantly change; however, CHOP expression was significantly induced with sorafenib treatment alone or in combination with SERCA inhibitors (Fig. 10F). In contrast, metastatic HCC cells showed high SERCA1 expression following treatment with sorafenib alone or in combination with SERCA inhibitors (Fig. 10G–I). Moreover, the sorafenib-induced overexpression of CHOP was significantly alleviated by an increase in SERCA1. However, the functional inhibition of SERCA1 using SERCA1-specific inhibitors, candidate 56 and 62 increased in acute ER stress (CHOP induction) (Fig. 10G–I). Candidate 56 and 62, administered alone did not significantly influence the hepatic injury of mice compare than carbon tetrachloride alone treatment (CCl_4, positive control) (Fig. 10J). Moreover, candidate 56 and 62-mediated cardiac injury was no significantly induced in mice (Fig. 10O–R).

The increase in SERCA1 in metastatic HCC represents a targetable mechanism to overcome resistance. Consequently, in metastatic HCC, CaMK2α-mediated SERCA1 increase becomes a pivotal factor for survival under acute ER stress. These new small molecules, the SERCA1-specific inhibitors candidate 56 and 62, present a promising therapeutic approach for unmet medical needs without causing side effects and could potentially treat patients with anti-cancer drug-resistant-mediated metastatic and recurrent cancer at lower doses than those required for individual anti-cancer drug use.

4. Discussion

The advancement of anti-cancer drugs has led to numerous studies demonstrating the benefits of preoperative treatments in enhancing survival rates post-surgery [35]. Despite this progress, there remains a lack of established therapeutic options as typical neoadjuvant or

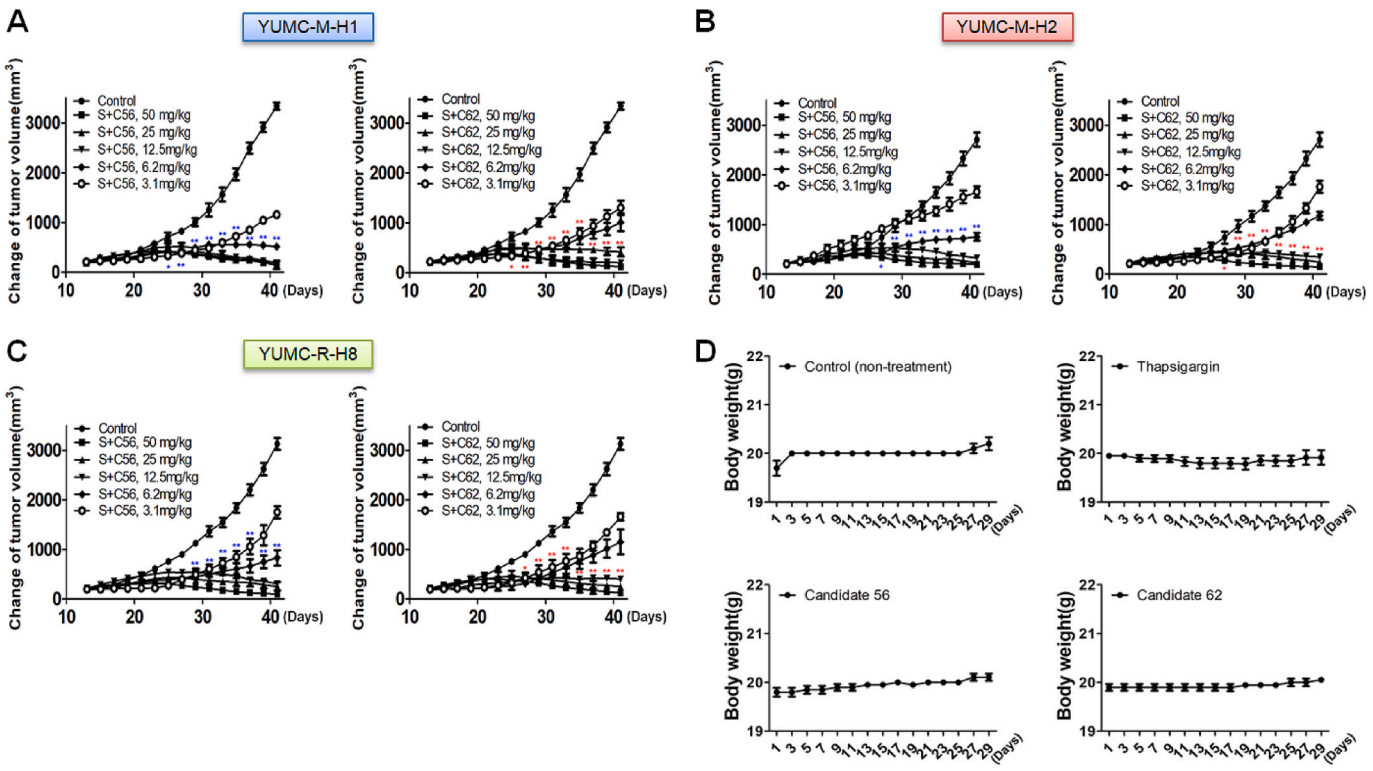

Fig. 9. Changes in relative tumor volumes at different doses of sorafenib A: YUMC-M−H1, B: YUMC-M−H2, C: YUMC-M−H3. The dose of candidate 56 or 62 was fixed 25 mg/kg (p.o.). Data are presented as mean ± standard error of mean. *p < 0.05 versus control (candidate 56 or 62 + 40 mg/kg sorafenib), **p < 0.01 versus control (candidate 56 or 62 + 40 mg/kg sorafenib). *,**; candidate 56, *,**; candidate 62. D, The change of whole body weight measurement under treatment with thapsigargin, candidate 56 or 62 alone in normal mice (not xenograft model) compared with the non-treated group.

adjuvant treatments for HCC [36,37], leading to a continual increase in unmet medical needs. A consequential portion of these unmet needs is caused to the recurrence and metastasis mediated by anti-cancer drug resistance [38]. Therefore, targeting anti-cancer drug resistant mediated-metastatic cancer cells remains a significant challenge in cancer treatment and research [39,40]. The mechanism of cancer metastasis in patients with cancer differs significantly for each cancer, owing to specific attributes that negatively affect cancer therapy and eventually cause cancer progression and death [40,41]. Consequently, a clinical intervention for anti-cancer drug resistant-mediated metastatic cancer is an unattainable target. In the current study, we postulated a therapeutic framework for metastatic cancer based on the results of a prototypical model experiment. The ultimate goal of anti-cancer drugs is to induce cancer cell death. However, anti-cancer drug resistant-mediated metastatic cancer cells evade death through epigenetic reprogramming, which upregulates numerous target genes [42]. Among the various mechanisms of evading cell death, refractory cancer could be resistant to ER stress by evading excess cytosolic free calcium-mediated apoptosis under anti-cancer drug treatment or glucose starvation metabolic stress [9] and phenocopy cytotoxic chemotherapy-resistant cancers [8,16,23]. Conventional anti-cancer drugs target the increase in cytosolic free calcium, which causes calcium-mediated apoptosis in anti-cancer drug-sensitive cancer cells [43]. Management of excess cytosolic free calcium is critical in apoptosis-resistant cancer cells and is facilitated by the calcium pump [14,17,18,44]. In refractory cancers like anti-cancer drug-resistant-mediated cancer cells many target genes are upregulated for survival under acute ER stress conditions [45]. SERCA is a critical target protein that supports low levels of resting cytosolic free calcium in cancer cells [46]. Moreover, enhanced SERCA expression is involved with poor outcomes in cancer, since it protects cells from excess overburdened cytosolic free calcium-mediated apoptosis [47].

The results of this study showed that, among the SERCA isoforms, SERCA1 levels predominantly increased in patient-derived metastatic HCC cells and further identified two novel small molecules, candidate 56 and 62, which were SERCA1-structure based specific inhibitors. mRNA sequencing (mRNA-Seq) analysis was based on the ECBS program, pharmacophore, and docking-oriented consecutive virtual screening for identifying novel SERCA1-specific inhibitors, to devise a therapeutic strategy for refractory cancer. mRNA-Seq and immunoblot analyses revealed higher SERCA1 expression in metastatic HCC cells than that in non-metastatic HCC cells. Kyoto Encyclopedia of Genes and Genomes (KEGG) pathway analysis showed that Calcium and Notch signaling pathways ranked high among the top 10 signaling pathways in patient-derived metastatic HCC cells compared to those in patient-derived non-metastatic HCC cells. The correlation between Notch and Calcium signaling pathways is well-established [48], and Notch signaling is managed by SERCA suppression [49]. Consequently, we identified SERCA isoforms and excess cytosolic free calcium-mediated apoptosis as key players in numerous upregulated target genes [50]. The present study findings revealed that enhanced SERCA1 transcription through NFκB nuclear translocation by CaMK2α plays a pivotal role in evading excess cytosolic free calcium mediated apoptosis under acute ER stress conditions in anti-cancer drug (sorafenib)-induced cytotoxic stress-resistant HCC cells. Increase in SERCA1 levels by CaMK2α enhances the restoration of excess cytosolic free calcium, which mainly contributes to anti-cancer drug-resistance-mediated metastasis to anti-cancer drug treatment-elevated acute ER stress. Increase in SERCA1 expression by CaMK2α restrains excess calcium-dependent apoptosis.

Notably, the current study proposes a reliable therapeutic approach for patient-derived metastatic HCC by identifying novel SERCA1-specific inhibitors, candidate 56 and 62. The present study findings validate the role of candidate 56 and 62, which could be prevent cardiac injury. SERCA isoforms are well-known key regulators of cardiac muscle, and therapeutic approaches to these SERCA inhibitors are unavoidably involved in cardiac dysfunction. Consequently, patients with SERCA-dependent anti-cancer drug-resistant-mediated metastatic

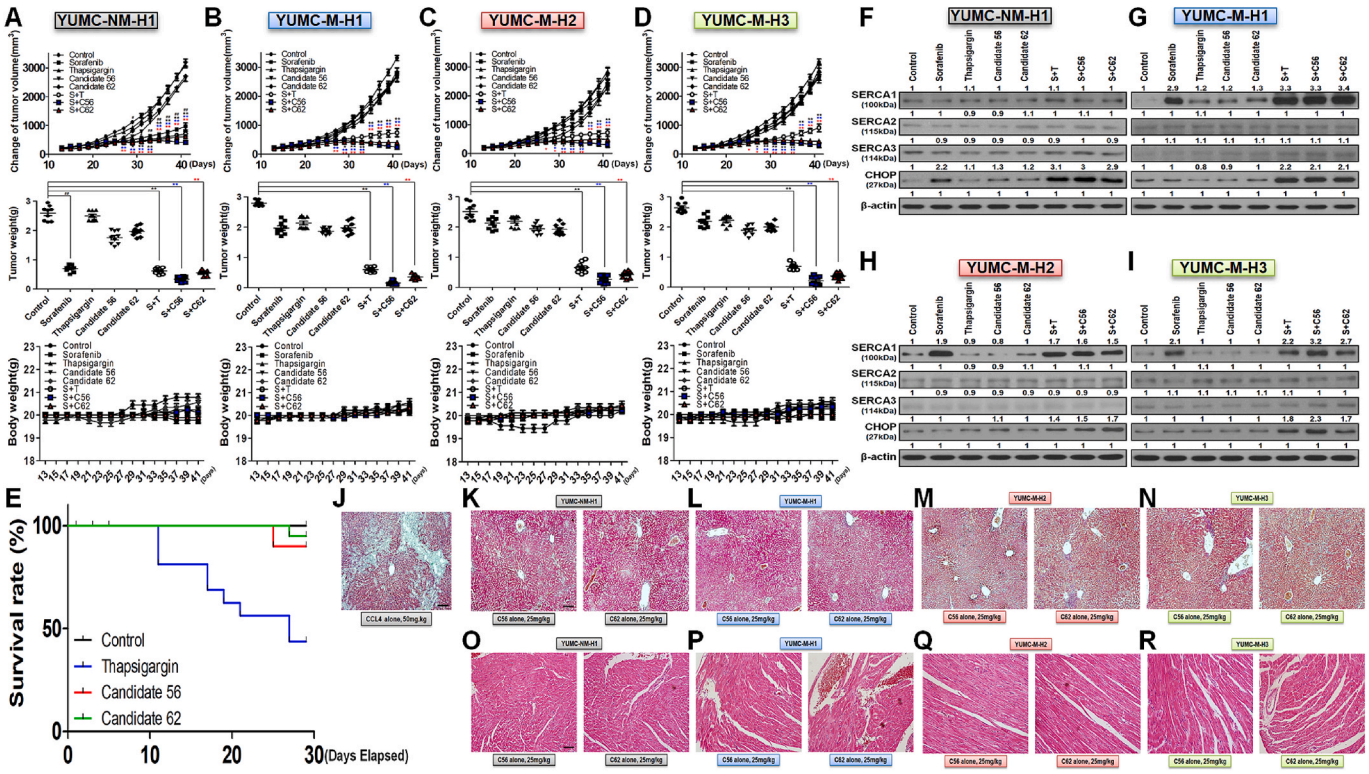

Fig. 10. Candidate 56 and 62 suppressed tumor growth in a xenograft model of patient-derived metastatic HCC cells. A, non-metastatic HCC cells (YUMC-NM-H1), B, C and D metastatic (YUMC-M−H1, –H2, and –H3) HCC cells, Changes in relative tumor volumes (top), resected tumor weights (middle), and whole body weights (bottom) of patient-derived HCC cells (each group, n = 10). Tumor sizes were calculated in NOD/Shi-scid, IL-2Rγ KOJic (NOG) mice. Animals were treated with each agent alone or sorafenib combined with the SERCA inhibitors, thapsigargin, candidate 56, and 62. Data represent the mean ± standard error of the mean. *.# $p < 0.05$ and **,## $p < 0.01$, compared with the control. #, ##; versus control, *,**; thapsigargin control, *,**; candidate 56, *,**; candidate 62, T; thapsigargin. E, The change of death ratio measurement under treatment with thapsigargin, candidate 56 or 62 alone in normal mice (not xenograft model) compared with the non-treated group (control). F–I, Immunoblot assay for the induction of SERCA isoforms (1–3) and ER stress under combination treatment SERCA1-specific inhibitors, candidate 56 and 62 with sorafenib in a mouse xenograft model with patient-derived non-metastatic and metastatic HCC cells. I–M and O–R, The histological change of the liver and heart similar treatment as shown by Masson's trichrome staining. Nuclei are stained black, cytoplasm and muscle fibres red, and ECM components blue. All slides were examined at 200 × magnification; scale bar: 100 μm. Each assay was performed in triplicate, and the representative images are presented. C56; candiate 56, C62; candidate 62. Each assay was performed at least in triplicate. (For interpretation of the references to colour in this figure legend, the reader is referred to the web version of this article.)

cancer may also be concerned about cardiac dysfunction. However, identification and validation of SERCA isoform-specific inhibitors, as in the current study, may potentially decrease cardiac dysfunction. Findings of current study might be positive to founding prospective, logical clinical approaches in patients with refractory HCC to advance efficacious theraphy. In a clinical relevance, these outcomes of current study impart consequential outcomes for the improvement of novel combined strategies and the discovery of new anti-cancer candidates that target a specific vulnerability of malignant cells, like drug resistant-mediated etastatic cancer cells. However, several further studies were needed to establish the present clinical approach. Additionally, more study is needed owing to the constraints of a few patient results. To overcome these constraints, several studies are on going on various types of patient-derived anti-cancer drug-resistant-mediated metastatic cancer.

4.1. Conclusions

In current study, we have first showed that SERCA1 expression by CaMK2α is fundamentally responsible for cellular resistance to cytotoxic stress induced by sorafenib treatment in patient-derived metastatic HCC model. Additionally, we suggest a therapeutic approach for prompting substantial tumor shrinkage in metastatic HCC cells using novel small molecules, candidate 56 and 62, which are SERCA1 isoform-specific inhibitors. The findings of this research hold promise for informing future therapeutic strategies aimed at enhancing efficacy in patients with refractory cancer. Clinically, these outcomes may have significant consequences for the improvement of new combinatorial therapies and the identification of novel anti-cancer candidates targeting specific vulnerabilities of malignant cells, such as anti-cancer drug resistant-mediated metastatic CSCs. However, further investigations are warranted to validate these therapeutic approaches. Nonetheless, targeting epigenetic changes between anti-cancer drug sensitive and −resistant cancers represents a pragmatic approach for managing patients with refractory cancers.

CRediT authorship contribution statement

Jin Hong Lim: Conceptualization, Data curation, Formal analysis, Investigation, Methodology, Resources, Software. **Keunwan Park:** Visualization, Validation, Software, Resources, Methodology, Formal analysis, Data curation. **Kyung Hwa Choi:** Writing – original draft, Visualization, Validation, Investigation, Conceptualization. **JungMin Kim:** Visualization, Validation, Software, Resources. **Yoo-Lim Jhe:** Formal analysis, Data curation, Conceptualization. **Seok-Mo Kim:** Visualization, Validation, Supervision, Software, Resources, Project administration, Methodology, Investigation, Formal analysis, Data curation. **Ki-Cheong Park:** Writing – review & editing, Writing – original draft, Visualization, Validation, Supervision, Software, Resources, Project administration, Methodology, Investigation, Funding acquisition, Formal analysis, Data curation, Conceptualization. **Jae-Ho**

Cheong: Writing – review & editing, Writing – original draft, Visualization, Validation, Supervision, Software, Resources, Project administration, Methodology, Investigation, Funding acquisition, Formal analysis, Data curation, Conceptualization.

Declaration of competing interest

The authors declare that they have no known competing financial interests or personal relationships that could have appeared to influence the work reported in this paper.

Acknowledgments

This study received support from a grant from the KHIDI, funded by the Ministry of Health & Welfare, Republic of Korea (HI18C1188), the Basic Science Research Program through the National Research Foundation of Korea (NRF), funded by the Ministry of Education (NRF-2017R1D1A1B03029716), and CKP Therapeutics, Inc. (grant numbers: 2021-31-1118), the Ministry of Trade, Industry & Energy (MOTIE), Korea Planning & Evaluation Institute of Industrial Technology (KEIT) through the Encouragement Program for Technology Development (Project NO: RS-2024-00410585). We thank proffesor Chan Wung Kim (CKP Therapeutics, Inc., Massachusetts Medical Device Development Center, 110 Canal Street, Lowell MA 01852, USA) for supporting this research. Particulary we extend our sincere gratitude to Mung-Kun Park and Hyun Joo Hwang for their invaluable support in this research.

Ethics approval and consent to participate

The research protocol was approved by the Institutional Review Board of Severance Hospital, Yonsei University College of Medicine (IRB Protocol: 3-2022-0331). Cell samples were obtained from patients at the Severance Hospital, Yonsei University College of Medicine, Seoul, Republic of Korea. This study was performed in accordance with the Declaration of Helsinki. The requirement for obtaining informed consent was waived owing to the retrospective nature of the study.

Data availability

All data generated or analyzed during this study are included in this published article or available from the corresponding author upon reasonable request.

References

[1] A. Alqahtani, Z. Khan, A. Alloghbi, T.S. Said Ahmed, M. Ashraf, D.M. Hammouda, Hepatocellular carcinoma: molecular mechanisms and targeted therapies, Medicina 55 (9) (2019), https://doi.org/10.3390/medicina55090526.
[2] B. Wei, W. Lou, Bioinformatic analysis shows the correlation of hsa_circ_0006220-miR-221/222-3p-ESR1/KDR axis with sorafenib resistance of hepatocellular carcinoma, Noncoding RNA Res 9 (1) (2024) 55–65, https://doi.org/10.1016/j.ncrna.2023.11.001.
[3] M. Ikeda, S. Mitsunaga, I. Ohno, Y. Hashimoto, H. Takahashi, K. Watanabe, et al., Systemic chemotherapy for advanced hepatocellular carcinoma: past, Present, and Future, Diseases 3 (4) (2015) 360–381, https://doi.org/10.3390/diseases3040360.
[4] T.C. Wu, Y.C. Shen, A.L. Cheng, Evolution of systemic treatment for advanced hepatocellular carcinoma, Kaohsiung J. Med. Sci. 37 (8) (2021) 643–653, https://doi.org/10.1002/kjm2.12401.
[5] J.M. Llovet, R. Montal, D. Sia, R.S. Finn, Molecular therapies and precision medicine for hepatocellular carcinoma, Nat. Rev. Clin. Oncol. 15 (10) (2018) 599–616, https://doi.org/10.1038/s41571-018-0073-4.
[6] B. Faubert, A. Solmonson, R.J. DeBerardinis, Metabolic reprogramming and cancer progression, Science 368 (6487) (2020), https://doi.org/10.1126/science.aaw5473.
[7] A. Deshmukh, K. Deshpande, F. Arfuso, P. Newsholme, A. Dharmarajan, Cancer stem cell metabolism: a potential target for cancer therapy, Mol. Cancer 15 (1) (2016) 69, https://doi.org/10.1186/s12943-016-0555-x.
[8] K.C. Park, J.M. Kim, S.Y. Kim, S.M. Kim, J.H. Lim, M.K. Kim, et al., PMCA inhibition reverses drug resistance in clinically refractory cancer patient-derived models, BMC Med. 21 (1) (2023) 38, https://doi.org/10.1186/s12916-023-02727-8.
[9] K.C. Park, S.W. Kim, J.Y. Jeon, A.R. Jo, H.J. Choi, J. Kim, et al., Survival of cancer stem-like cells under metabolic stress via CaMK2alpha-mediated upregulation of sarco/endoplasmic reticulum calcium ATPase expression, Clin. Cancer Res. 24 (7) (2018) 1677–1690, https://doi.org/10.1158/1078-0432.CCR-17-2219.
[10] L. Chen, Y. Qin, B. Liu, M. Gao, A. Li, X. Li, et al., PGC-1alpha-mediated mitochondrial quality control: molecular mechanisms and implications for heart failure, Front. Cell Dev. Biol. 10 (2022) 871357, https://doi.org/10.3389/fcell.2022.871357.
[11] S. Marchi, S. Patergnani, S. Missiroli, G. Morciano, A. Rimessi, M.R. Wieckowski, et al., Mitochondrial and endoplasmic reticulum calcium homeostasis and cell death, Cell Calcium 69 (2018) 62–72, https://doi.org/10.1016/j.ceca.2017.05.003.
[12] F. Giamogante, E. Poggio, L. Barazzuol, A. Covallero, T. Cali, Apoptotic signals at the endoplasmic reticulum-mitochondria interface, Adv. Protein Chem. Struct. Biol. 126 (2021) 307–343, https://doi.org/10.1016/bs.apcsb.2021.02.007.
[13] A. Tripathi, S.K. Chaube, High cytosolic free calcium level signals apoptosis through mitochondria-caspase mediated pathway in rat eggs cultured in vitro, Apoptosis : an International Journal on Programmed Cell Death 17 (5) (2012) 439–448, https://doi.org/10.1007/s10495-012-0702-9.
[14] Y. Kim, H.J. Yun, K.H. Choi, C.W. Kim, J.H. Lee, R. Weicker, et al., Discovery of new anti-cancer agents against patient-derived sorafenib-resistant papillary thyroid cancer, Int. J. Mol. Sci. 24 (22) (2023), https://doi.org/10.3390/ijms242216413.
[15] G.R. Monteith, F.M. Davis, S.J. Roberts-Thomson, Calcium channels and pumps in cancer: changes and consequences, J. Biol. Chem. 287 (38) (2012) 31666–31673, https://doi.org/10.1074/jbc.R112.343061.
[16] S.M. Kim, S.Y. Kim, C.S. Park, H.S. Chang, K.C. Park, Impact of age-related genetic differences on the therapeutic outcome of papillary thyroid cancer, Cancers 12 (2) (2020), https://doi.org/10.3390/cancers12020448.
[17] J.H. Lim, K. Park, K.H. Choi, C.W. Kim, J.H. Lee, R. Weicker, et al., Drug discovery using evolutionary similarities in chemical binding to inhibit patient-derived hepatocellular carcinoma, Int. J. Mol. Sci. 23 (14) (2022), https://doi.org/10.3390/ijms23147971.
[18] H.S. Chang, Y. Kim, S.Y. Lee, H.J. Yun, H.J. Chang, K.C. Park, Anti-cancer SERCA inhibitors targeting sorafenib-resistant human papillary thyroid carcinoma, Int. J. Mol. Sci. 24 (8) (2023), https://doi.org/10.3390/ijms24087069.
[19] L. Zhihao, N. Jingyu, L. Lan, S. Michael, G. Rui, B. Xiyun, et al., SERCA2a: a key protein in the Ca(2+) cycle of the heart failure, Heart Fail. Rev. 25 (3) (2020) 523–535, https://doi.org/10.1007/s10741-019-09873-3.
[20] J. Palomeque, M.V. Petroff, L. Sapia, O.A. Gende, C. Mundina-Weilenmann, A. Mattiazzi, Multiple alterations in Ca2+ handling determine the negative staircase in a cellular heart failure model, J. Card. Fail. 13 (2) (2007) 143–154, https://doi.org/10.1016/j.cardfail.2006.11.002.
[21] D. Kim, B. Langmead, S.L. Salzberg, HISAT: a fast spliced aligner with low memory requirements, Nat. Methods 12 (4) (2015) 357–360, https://doi.org/10.1038/nmeth.3317.
[22] M. Pertea, D. Kim, G.M. Pertea, J.T. Leek, S.L. Salzberg, Transcript-level expression analysis of RNA-seq experiments with HISAT StringTie and Ballgown, Nature Protocols 11 (9) (2016) 1650–1667, https://doi.org/10.1038/nprot.2016.095.
[23] J.H. Lim, K.H. Choi, S.Y. Kim, C.S. Park, S.M. Kim, K.C. Park, Patient-derived, drug-resistant colon cancer cells evade chemotherapeutic drug effects via the induction of epithelial-mesenchymal transition-mediated angiogenesis, Int. J. Mol. Sci. 21 (20) (2020), https://doi.org/10.3390/ijms21207469.
[24] J. Jumper, R. Evans, A. Pritzel, T. Green, M. Figurnov, O. Ronneberger, et al., Highly accurate protein structure prediction with AlphaFold, Nature 596 (7873) (2021) 583–589, https://doi.org/10.1038/s41586-021-03819-2.
[25] L.G. Nivon, R. Moretti, D. Baker, A Pareto-optimal refinement method for protein design scaffolds, PLoS One 8 (4) (2013) e59004, https://doi.org/10.1371/journal.pone.0059004.
[26] K.W. Kaufmann, J. Meiler, Using RosettaLigand for small molecule docking into comparative models, PLoS One 7 (12) (2012) e50769, https://doi.org/10.1371/journal.pone.0050769.
[27] C. Mauro, S.C. Leow, E. Anso, S. Rocha, A.K. Thotakura, L. Tornatore, et al., NF-kappaB controls energy homeostasis and metabolic adaptation by upregulating mitochondrial respiration, Nat. Cell Biol. 13 (10) (2011) 1272–1279, https://doi.org/10.1038/ncb2324.
[28] J.A. Seo, B. Kim, D.N. Dhanasekaran, B.K. Tsang, Y.S. Song, Curcumin induces apoptosis by inhibiting sarco/endoplasmic reticulum Ca2+ ATPase activity in ovarian cancer cells, Cancer Lett. 371 (1) (2016) 30–37, https://doi.org/10.1016/j.canlet.2015.11.021.
[29] C. Cui, R. Merritt, L. Fu, Z. Pan, Targeting calcium signaling in cancer therapy, Acta Pharm. Sin. B 7 (1) (2017) 3–17, https://doi.org/10.1016/j.apsb.2016.11.001.
[30] L. Qian, Y. Zhu, C. Deng, Z. Liang, J. Chen, Y. Chen, et al., Peroxisome proliferator-activated receptor gamma coactivator-1 (PGC-1) family in physiological and pathophysiological process and diseases, Signal Transduct. Target. Ther. 9 (1) (2024) 50, https://doi.org/10.1038/s41392-024-01756-w.
[31] K. Park, Y.J. Ko, P. Durai, C.H. Pan, Machine learning-based chemical binding similarity using evolutionary relationships of target genes, Nucleic Acids Res. 47 (20) (2019) e128.
[32] M. van Kempen, S.S. Kim, C. Tumescheit, M. Mirdita, J. Lee, C.L.M. Gilchrist, et al., Fast and accurate protein structure search with Foldseek, Nat. Biotechnol. 42 (2) (2024) 243–246, https://doi.org/10.1038/s41587-023-01773-0.
[33] K. El Omari, N. Mohamad, K. Bountra, R. Duman, M. Romano, K. Schlegel, et al., Experimental phasing with vanadium and application to nucleotide-binding membrane proteins, IUCrJ 7 (Pt 6) (2020) 1092–1101, https://doi.org/10.1107/S2052252520012312.

[34] O. Rodriguez-Mora, M.M. LaHair, C.J. Howe, J.A. McCubrey, R.A. Franklin, Calcium/calmodulin-dependent protein kinases as potential targets in cancer therapy, Expert Opin. Ther. Targets 9 (4) (2005) 791–808, https://doi.org/10.1517/14728222.9.4.791.
[35] A.J. Kerr, D. Dodwell, P. McGale, F. Holt, F. Duane, G. Mannu, et al., Adjuvant and neoadjuvant breast cancer treatments: a systematic review of their effects on mortality, Cancer Treat. Rev. 105 (2022) 102375, https://doi.org/10.1016/j.ctrv.2022.102375.
[36] C. Akateh, S.M. Black, L. Conteh, E.D. Miller, A. Noonan, E. Elliott, et al., Neoadjuvant and adjuvant treatment strategies for hepatocellular carcinoma, World J. Gastroenterol. 25 (28) (2019) 3704–3721, https://doi.org/10.3748/wjg.v25.i28.3704.
[37] F. Foerster, P.R. Galle, The current landscape of clinical trials for systemic treatment of HCC, Cancers (Basel) 13 (2021), https://doi.org/10.3390/cancers13081962.
[38] N. Vasan, J. Baselga, D.M. Hyman, A view on drug resistance in cancer, Nature 575 (7782) (2019) 299–309, https://doi.org/10.1038/s41586-019-1730-1.
[39] B. Du, J.S. Shim, Targeting epithelial-mesenchymal transition (EMT) to overcome drug resistance in cancer, Molecules 21 (7) (2016), https://doi.org/10.3390/molecules21070965.
[40] E.J. Kilmister, S.P. Koh, F.R. Weth, C. Gray, S.T. Tan, Cancer metastasis and treatment resistance: mechanistic insights and therapeutic targeting of cancer stem cells and the tumor microenvironment, Biomedicines 10 (11) (2022), https://doi.org/10.3390/biomedicines10112988.
[41] M. Nedeljkovic, A. Damjanovic, Mechanisms of chemotherapy resistance in triple-negative breast cancer-how we can rise to the challenge, Cells 8 (9) (2019), https://doi.org/10.3390/cells8090957.
[42] N. Duan, Y. Hua, X. Yan, Y. He, T. Zeng, J. Gong, et al., Unveiling alterations of epigenetic modifications and chromatin architecture leading to lipid metabolic reprogramming during the evolutionary trastuzumab adaptation of HER2-positive breast cancer, Adv. Sci. 11 (18) (2024) e2309424, https://doi.org/10.1002/advs.202309424.
[43] E. Varghese, S.M. Samuel, Z. Sadiq, P. Kubatka, A. Liskova, J. Benacka, et al., Anti-cancer agents in proliferation and cell death: the calcium connection, Int. J. Mol. Sci. 20 (12) (2019), https://doi.org/10.3390/ijms20123017.
[44] S.M. Kim, K. Park, J.H. Lim, H.J. Yun, S.Y. Kim, K.H. Choi, et al., Potential therapeutic agents against paclitaxel-and sorafenib-resistant papillary thyroid carcinoma, Int. J. Mol. Sci. 23 (18) (2022), https://doi.org/10.3390/ijms231810378.
[45] D. Xu, Z. Liu, M.X. Liang, Y.J. Fei, W. Zhang, Y. Wu, et al., Endoplasmic reticulum stress targeted therapy for breast cancer, Cell Commun. Signal 20 (1) (2022) 174, https://doi.org/10.1186/s12964-022-00964-7.
[46] E.R. Chemaly, L. Troncone, D. Lebeche, SERCA control of cell death and survival, Cell Calcium 69 (2018) 46–61, https://doi.org/10.1016/j.ceca.2017.07.001.
[47] S. Zheng, X. Wang, D. Zhao, H. Liu, Y. Hu, Calcium homeostasis and cancer: insights from endoplasmic reticulum-centered organelle communications, Trends Cell Biol. 33 (4) (2023) 312–323, https://doi.org/10.1016/j.tcb.2022.07.004.
[48] N. Saini, S. Lakshminarayanan, P. Kundu, A. Sarin, Notch1 modulation of cellular calcium regulates mitochondrial metabolism and anti-apoptotic activity in T-regulatory cells, Front. Immunol. 13 (2022) 832159, https://doi.org/10.3389/fimmu.2022.832159.
[49] L. Pagliaro, M. Marchesini, G. Roti, Targeting oncogenic Notch signaling with SERCA inhibitors, J. Hematol. Oncol. 14 (1) (2021) 8, https://doi.org/10.1186/s13045-020-01015-9.
[50] S.M. Kim, K. Park, H.J. Yun, J.M. Kim, K.H. Choi, K.C. Park, Identification of new small molecules for selective inhibition of SERCA 1 in patient-derived metastatic papillary thyroid cancer, Br. J. Pharmacol. 182 (11) (2025) 2392–2408, https://doi.org/10.1111/bph.17442.